AFRL-VS-HA-TR-98-0085

DETECTION OF RIPPLE FIRING IN TIME AND FREQUENCY

Robert H. Shumway

University of California
Division of Statistics
Davis, CA 95616

30 December 1997

Final Scientific Report

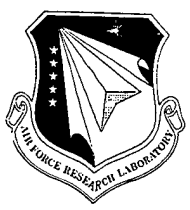

PHILLIPS LABORATORY
Directorate of Geophysics
AIR FORCE MATERIEL COMMAND
HANSCOM AFB, MA 01731-3010

SPONSORED BY
Air Force Technical Applications Center
Directorate of Nuclear Treaty Monitoring
Project Authorization T/5101

MONITORED BY
Air Force Research Laboratory
CONTRACT No. F19628-95-K-0010

The views and conclusions contained in this document are those of the authors and should not be interpreted as representing the official policies, either express or implied, of the Air Force or U.S. Government.

This technical report has been reviewed and is approved for publication.

JAMES C. BATTIS
Contract Manager

CHARLES P. PIKE, Chief
Technology Outreach Branch

This report has been reviewed by the ESD Public Affairs Office (PA) and is releasable to the National Technical Information Service (NTIS).

Qualified requestors may obtain copies from the Defense Technical Information Center. All others should apply to the National Technical Information Service.

If your address has changed, or you wish to be removed from the mailing list, or if the addressee is no longer employed by your organization, please notify AFRL/VSOS-IM, 29 Randolph Road, Hanscom AFB, MA 01731-3010. This will assist us in maintaining a current mailing list.

Do not return copies of the report unless contractual obligations or notices on a specific document requires that it be returned.

REPORT DOCUMENTATION PAGE

Form Approved
OMB No. 0704-0188

1. AGENCY USE ONLY (Leave blank)	2. REPORT DATE	3. REPORT TYPE AND DATES COVERED
	30 Dec. 1997	Final Report 9/1/94 - 9/30/97

4. TITLE AND SUBTITLE
Detection of Ripple-Firing in Time and Frequency

5. FUNDING NUMBERS
F19628-95-K-0010
PE:
PR 5101
TA GM
WU AL

6. AUTHOR(S)
Robert H. Shumway

7. PERFORMING ORGANIZATION NAME(S) AND ADDRESS(ES)
Division of Statistics
University of California
One Shields Avenue
Davis CA 95616

8. PERFORMING ORGANIZATION REPORT NUMBER
Division of Statistics
Technical Report # 332

9. SPONSORING/MONITORING AGENCY NAME(S) AND ADDRESS(ES)
Phillips Laboratory
29 Randolph Road
Hanscom AFB, MA 01731-3010

10. SPONSORING/MONITORING AGENCY REPORT NUMBER
AFRL-VS-HA-TR-98-0085

11. SUPPLEMENTARY NOTES
Sponsored by Air Force Technical Applications Center, Directorate of Nuclear Treaty Monitoring. Issued by Phillips Laboratory under Contract F19628-95-K-0010.

12a. DISTRIBUTION/AVAILABILITY STATEMENT
Approved for public release; distribution unlimited.

12b. DISTRIBUTION CODE

13. ABSTRACT *(Maximum 200 words)*

Frequency and time domain approaches to detecting ripple firing on an array are developed and tested on simulated data and on 10 mining explosions in a quarry on Kola peninsula. The approaches are useful for isolating the periodic modulations in the spectra that may distinguish the signatures of mining explosions from those of earthquakes. All three methodologies exploit the assumption that approximately the same pattern should appear on all sensors after path and site effects have been eliminated.

In the first frequency domain method an additive noise model is used to deconvolve the common signal from path and site effects. A cepstral analysis exhibits the delay structure. In the second frequency domain method, a multiplicative convolution model is used to derive a Cepstral F-Statistic, based on the stacked cepstra and the spectrum of the stacked log spectra. The time domain approach involves searching the multiplicative convolution model using seasonal ARMA models for the delay structure and the source.

It is shown that all three approaches work reasonably well on contrived data but that frequency domain versions tend to be superior. The methods are then applied to four phases from 10 mining explosions on Kola, observed on 5 elements of the Norwegian array ARCESS. We conclude that some phases show evidence of rippling in the 100-200 millisecond range for all ten explosions.

14. SUBJECT TERMS
Mining explosions, Cepstral F, Deconvolution, Seasonal ARMA

15. NUMBER OF PAGES
45

16. PRICE CODE

17. SECURITY CLASSIFICATION OF REPORT	18. SECURITY CLASSIFICATION OF THIS PAGE	19. SECURITY CLASSIFICATION OF ABSTRACT	20. LIMITATION OF ABSTRACT
unclassified	unclassified	unclassified	SAR

TABLE OF CONTENTS

1. Introduction 1

2. Multiple Deconvolution 5

3. Seasonal Multiplicative ARMA Models for Arrays 9

4. The Nonlinear Cepstral F Detector 13

5. Analysis of Kola Mining Explosions 18

6. Discussion 21

7. References 23

Appendix A: Cepstral Analyses of Kola Peninsula Events 25

FIGURES IN TEXT

Figure 1: Mine Blast 110 from HD9 Quarry on Kola Observed at ARCESS and the Extracted P_n Phase (40 pts per second).....2

Figure 2: A Contrived Array With Delay Firing (d=8,15,23,30) and the Associated Detrended Log Spline Spectra.....7

Figure 3: The Bank of Deconvolution Filters (Left) With Deconvolved Signal (Top Right) and Cepstrum of Deconvolved Signal (Bottom Right) 8

Figure 4: BIC Contours for Seasonal ARMA Search Using Contrived Data. The darkest value corresponds to the minimum. The bottom panel averages BIC over the number of reflections and shows a consistent delay at $d = 8$ points.....12

Figure 5: Bank of Detrended Log Spectra (Right) and the Cepstral F-Statistic Showing Peaks at 8, 16, 23 and 30 points.....15

FIGURES IN APPENDIX A

Figure A1: Cepstral Analysis of Deconvolved Array Signal for Four Phases From Event 054 (Delay in points). 26

Figure A2: Cepstral F-Statistic for Four Phases From Event 054. 27

Figure A3: Cepstral Analysis of Deconvolved Array Signal for Four Phases From Event 066 (Delay in points). 28

Figure A4: Cepstral F-Statistic for Four Phases From Event 066 29

Figure A5: Cepstral Analysis of Deconvolved Array Signal for Four Phases From Event 110 (Delay in points). 30

Figure A6: Cepstral F-Statistic for Four Phases From Event 110 31

Figure A7: Cepstral Analysis of Deconvolved Array Signal for Four Phases From Event 138 (Delay in points). 32

Figure A8: Cepstral F-Statistic for Four Phases From Event 138 33

Figure A9: Cepstral Analysis of Deconvolved Array Signal for Four Phases From Event 147 (Delay in points). 34

Figure A10: Cepstral F-Statistic for Four Phases From Event 147 35

Figure A11: Cepstral Analysis of Deconvolved Array Signal for Four Phases From Event 182 (Delay in points). 36

Figure A12: Cepstral F-Statistic for Four Phases From Event 182 37

Figure A13: Cepstral Analysis of Deconvolved Array Signal for Four Phases From Event 219 (Delay in points). 38

Figure A14: Cepstral F-Statistic for Four Phases From Event 219. 39

Figure A15: Cepstral Analysis of Deconvolved Array Signal for Four Phases From Event 246 (Delay in points). 40

Figure A16: Cepstral F-Statistic for Four Phases From Event 246. 41

Figure A17: Cepstral Analysis of Deconvolved Array Signal for Four Phases From Event 282 (Delay in points). 42

Figure A18: Cepstral F-Statistic for Four Phases From Event 282. 43

Figure A19: Cepstral Analysis of Deconvolved Array Signal for Four Phases From Event 285 (Delay in points). 44

Figure A20: Cepstral F-Statistic for Four Phases From Event 285. 45

1. Introduction

Regional seismic monitoring and discrimination capabilities that are desirable under a potential Comprehensive Test Ban Treaty (CTBT) can be improved by developing new algorithms and procedures for distinguishing between earthquakes, nuclear explosions and mining explosions of various kinds. Much effort in past discrimination studies has concentrated on extracting various features of the spectrum that are characteristic of earthquakes, nuclear explosions or mine blasts.

One particular spectral feature that characterizes some mining explosions is a modulation of the spectrum introduced by a ripple-fired explosion. A ripple-fired event usually involves detonation of a number of explosions that are often regularly grouped in space and time. Such explosions, known as quarry blasts, have low magnitudes that may be close to those of nuclear explosions that one might monitor under the CTBT. As examples of these kinds of mine blasts, we consider using array data from the Arctic Experimental Seismic Station (ARCESS) in northern Norway, previously analyzed by Der et al (1993). The top panel of Figure 1 shows a single channel from a typical mine blast, sampled at 40 points per second, with four arrival phases identified. The arrival phases shown correspond to *body waves*, which are subdivided into compressional *P-waves*, denoted here by P_n and P_g, and shear *S-waves*, denoted by S_n and L_g. At regional distances, P_n is usually the first to arrive, having traveled down through the crust and then horizontally near the top of the upper mantle. P_g is a wave that comes in later than P_n, and travels the path between source and receiver wholly within the Earth's crust. S_n is a shear wave that travels a path similar to that of P_n but arrives later because shear waves propagate slower than the P-waves that make up P_n. L_g is a type of guided shear wave that has most of its energy trapped in the Earth's crust. In the bottom panel, we show the first arrival phase at all five channels.

The pattern induced by the delay-firing that is characteristic of mining activity can be represented in terms of a model that contains a signal $s(t)$ and its echoes, observed at a set of time delays, say $\tau_1, \tau_2, \ldots, \tau_n$, producing a theoretical output of the form

$$x(t) = s(t) + \sum_{j=1}^{n} \theta_j s(t - \tau_j), \tag{1}$$

where the initial signal $s(t)$ appears at the set of time delays indicated, with amplitudes $\theta_1, \theta_2, \ldots, \theta_n$. Identifying the length of the time delays for arrival phases as well as their configuration will be helpful for distinguishing ripple-fired patterns from those due to path

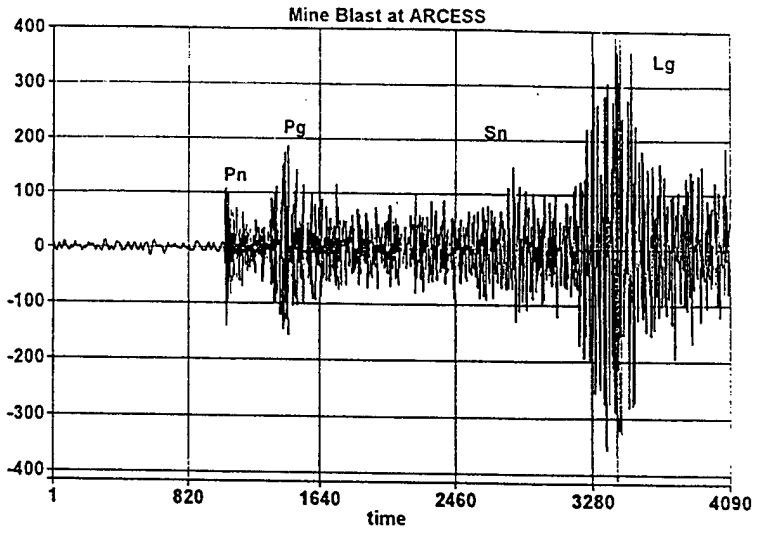

Stacked plot of PN110 Signal

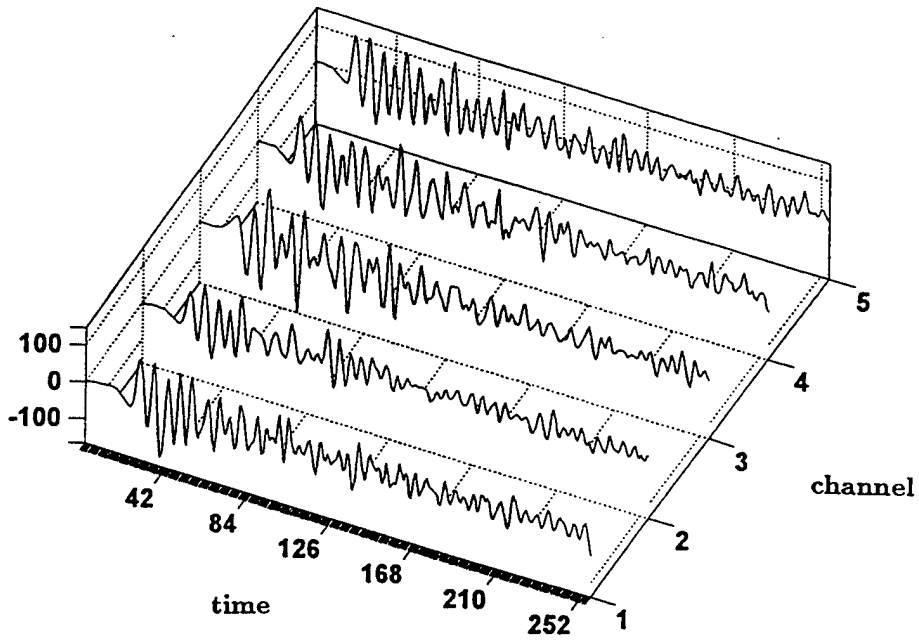

Figure 1: Mine Blast 110 from HD9 Quarry on Kola Observed at ARCESS and the Extracted P_n Phase (40 pts per second).

effects or local reverberations. A number of authors have examined various aspects of this problem and have proposed techniques for analyzing these ripple-fired seismic signals. Chapman et al (1992) show reflection patterns for a number of delay-fired configurations and propose a cepstral deconvolution method for estimating the delays. Baumgardt and Ziegler (1988) consider lining up the log-spectra and cepstra for an array and looking for common reflection patterns. Alexander et al (1995) extend this analysis by adding up or *stacking* the cepstra. Hedlin et al (1990) propose graphical techniques involving threshold modifications of the time varying log-spectra and cepstra. During the course of this project, we have developed three different approaches based on two different signal and noise models. They are:

(i) deconvolution of a common signal on an array (see Shumway and Der, 1985, Der et al, 1987, 1992, 1993), assuming an additive noise model, followed by a cepstral analysis of the deconvolved signal,

(ii) a search through Box-Jenkins seasonal autoregressive moving average (ARMA) models with parameters equal to the duration and time delays in a multiplicative signal and noise model

and

(iii) a nonlinear cepstral F-statistic (see Shumway et al, 1997) based on a frequency domain multiplicative model for the signals and noises. The approach formalizes ideas of Alexander et al (1995) and Baumgardt and Ziegler (1988) that are based on the premise that a common reflection pattern should appear at each channel on the array.

The deconvolution approach in (i) uses an additive linear model for the observed series at the jth sensor in an array, say $y_j(t), j = 1, 2, \ldots, N$ that takes the form

$$y_j(t) = a_j(t) \otimes x(t) + n_j(t), \tag{2}$$

where the notation $\otimes$ denotes convolution and the impulse-response functions $a_j(t)$ are used to denote the path and receiver effects that distinguish the jth element of the array from others. It will be assumed that these functions have relatively smooth Fourier transforms so that they can be estimated from the spectra of the observed series. We assume throughout that the signal and noise are stationary and independent of each other. Given reasonable estimators for the path and receiver transforms, the multiple deconvolution procedure of Shumway and Der (1985) is used to develop the deconvolution estimator for the common function $x(t)$. Then, because of (1), we may use the cepstral analysis procedure of Bogert,

Healy and Tukey (1962), denoted by BHT in the sequel, to estimate the time delays for the ripple firing. Section 2 gives details.

It is also possible to consider a multiplicative noise model of the form

$$y_j(t) = a_j(t) \otimes x(t) \otimes n_j(t) \tag{3}$$

as an alternate representation, leading to procedures (ii) and (iii) mentioned above. A simplification of (3) with equal receiver effects and delays $\tau_j = jd, j = 1, 2, \ldots, n$ proportional to some underlying delay d allows recasting (3) as a seasonal autoregressive model of the form considered in the classic work of Box and Jenkins (see Box, Jenkins and Reinsel, 1994 for expository material). The delays are the seasonal periods and the duration or number of reflections corresponds to the order of the seasonal moving average term. A low-order autoregressive component models the combined effects of source, path and instrument response. Seasonal ARMA models are searched over a number of plausible delays and duration, with the best value of a Bayesian information criterion (BIC) due to Schwarz (1978) used to select the best model. This approach is covered in Section 3.

Finally, the Fourier decomposition of the observed spectrum in the multiplicative model (3) suggests Method (iii) above. In this approach, the observed spectrum is expressed as a product of signal and noise spectra and Fourier transforms. Taking logarithms yields an additive model in the logarithms of the squared Fourier transforms that we can use as a model for detecting a common set of periodic components on an array of suitably detrended log-spectra. In our approach, assuming a multiplicative noise model, detrended log-spectra are derived as realizations of stationary processes whose periodic signal components are frequencies, with periods proportional to delay time differences. Using an approach proposed by Shumway (1971) for detecting a common signal in a collection of stationarily correlated series, an F-Statistic is derived that is proportional to the *stacked cepstrum* and the *spectrum of the stacked log-spectra.* Advantages of this cepstral F-Statistic stem from its superior resolving power and the fact that statistical significance can now be asserted for selected delay peaks.

Simulated array data and data involving four phases extracted from ten Kola mining explosions, measured at ARCESS in Scandinavia, are used to compare the time and frequency domain approaches. We cover the three methodologies in Sections 2, 3 and 4 and the data analysis in Section 5.

2. Multiple Deconvolution

The primary aim of the multiple deconvolution procedure is to isolate a reasonable estimator for the unobserved stationary process $x(t)$ in the additive model (2). This problem is somewhat different than single channel deconvolution, where there is only one realization for the signal $x(t)$. In what follows, we suppose that the spectra of the signal and noise processes are denoted by $P_s(\nu)$ and $P_n(\nu)$ respectively with ν, $-1/2 \leq \nu \leq 1/2$ defined as frequency in cycles per point. We assume the signal to noise ratio to be known, so there are no parameters to be estimated by maximum likelihood (see, for example, Hannan and Thomson, 1974 and Shumway, 1988 for approaches that develop parametric and non-parametric estimators for the signal and noise spectra). In the present case, it is possible to show (see Shumway, 1988) that the optimal deconvolution estimator for $x(t)$ is of the form

$$\hat{x}(t) = \sum_{j=1}^{N} h_j(t) \otimes y_j(t) \tag{4}$$

where $h_j(t)$ are filters applied at each sensor, with frequency response functions determined as

$$H_j(\nu) = \frac{A_j^*(\nu)}{\sum_{j=1}^{N} |A_j(\nu)|^2 + \delta^2(\nu)}, \tag{5}$$

where $\delta^2(\nu) = P_n(\nu)/P_x(\nu)$ and $A_j(\nu)$ is the Fourier transform of $a_j(t)$. Since the signal and noise spectra are somewhat complicated, as shown in the next paragraph, we use a small ridge correction $\delta^2(\nu) = \delta^2$, assumed to be constant over frequency, with the constant taking the role of the usual regularization parameter used to stabilize solutions to poorly conditioned inverse problems. The resulting estimator, $\hat{x}(t)$, should consist of the common components of all array elements and should be free of the effects of the path and receiver. Note that we still must know values for the frequency response functions $A_j(\nu)$; we discuss this problem later.

Now, from (1), the spectrum of $x(t)$ is given by

$$P_x(\nu) = |\theta(\nu)|^2 P_s(\nu), \tag{6}$$

with

$$|\theta(\nu)|^2 = \sum_{j=0}^{n} \sum_{k=0}^{n} \theta_j \theta_k \cos[2\pi\nu(\tau_j - \tau_k)], \tag{7}$$

($\theta_0 = 1$) which is the component introduced by the possible ripple firing. BHT(1962) noted that the squared transfer function (7) will be periodic, with components proportional to

the time delay differences. For multiplicative models like (6), BHT proposed an additive model, obtained by transforming to logarithms. For a sample series $x(t), t = 0, 1, \ldots, T-1$ and discrete frequencies of the form $\nu_\ell = \ell/T, \ell = 0, 1, \ldots, T/2$, the log spectrum can be written as

$$\log P_x(\nu_\ell) = \log |\theta(\nu_\ell)|^2 + \log P_s(\nu_\ell). \tag{8}$$

BHT noted that the first component will be periodic, with frequencies proportional to $T/(\tau_j - \tau_k), j, k = 1, \ldots, n$ and proposed computing the spectrum of (8), called the *cepstrum* which should exhibit the periodicities in (8) as cepstral peaks.

The results given above suggest deconvolving on the array to get the estimator for $\hat{x}(t)$ and then computing the cepstrum of the deconvolved series to isolate the periodicities. As mentioned before, the success of the procedure will depend on finding reasonable estimators for the receiver response functions $A_j(\nu)$. To do this, we note that the spectrum of the received signal in (3) will be

$$P_{y_j}(\nu) = |A_j(\nu)|^2 P_x(\nu) + P_n(\nu). \tag{9}$$

We suppose, furthermore, that the noise spectrum can be neglected in (9) and that the function $A_j(\nu)$ is reasonably smooth over frequency. Consider the cubic spline approximation

$$\log |A_j(\nu_\ell)|^2 + \log P_x(\nu) \approx a_{j0} + a_{j1}\nu_\ell + a_{j2}\nu_\ell^2 + \hat{a}_{j3}\nu_\ell^3 + \hat{a}_{j4}(\nu_\ell - \nu_f)_+^3, \tag{10}$$

where ν_f is the knot location and $(\nu - \nu_f)_+^3$ for $\ell = 0, 1, \ldots, T/2$. The spline approximation with one knot should be smooth enough so that the residuals from the fitted spline will still retain the periodic components in $|\theta(\nu)|^2$ that correspond to the ripple fired signal. The resulting approximation (10) for the smooth part of $\log |A_j(\nu)|^2$ can be exponentiated and the positive square root of the result used as the frequency response function $A_j(\nu)$.

To illustrate some of the above ideas, consider the simulated ensemble of signals shown in the top panel of Figure 2. We generated different second-order autoregressive processes with a frequency content comparable to the seismic waveform in Figure 1 and modulated them with a fixed exponentially decaying function that emulates a transient signal. The results were added together at time delays $\tau_0 = 0, \tau_1 = 8, \tau_2 = 15, \tau_3 = 23, \tau_4 = 31$ with amplitudes $\theta_0 = 1, \theta_1 = .9, \theta_2 = .9, \theta_3 = .6, \theta_4 = .7$ to simulate a typical realization, according to (1). The five resulting series, shown in Figure 2, all contain the slightly different signals, at the same set of delays and we can argue that the model given by (1) and (2) is plausible and that any method based on the model should work reasonably well. A typical observed spectrum is shown in the bottom panel of Figure 2 and we note that

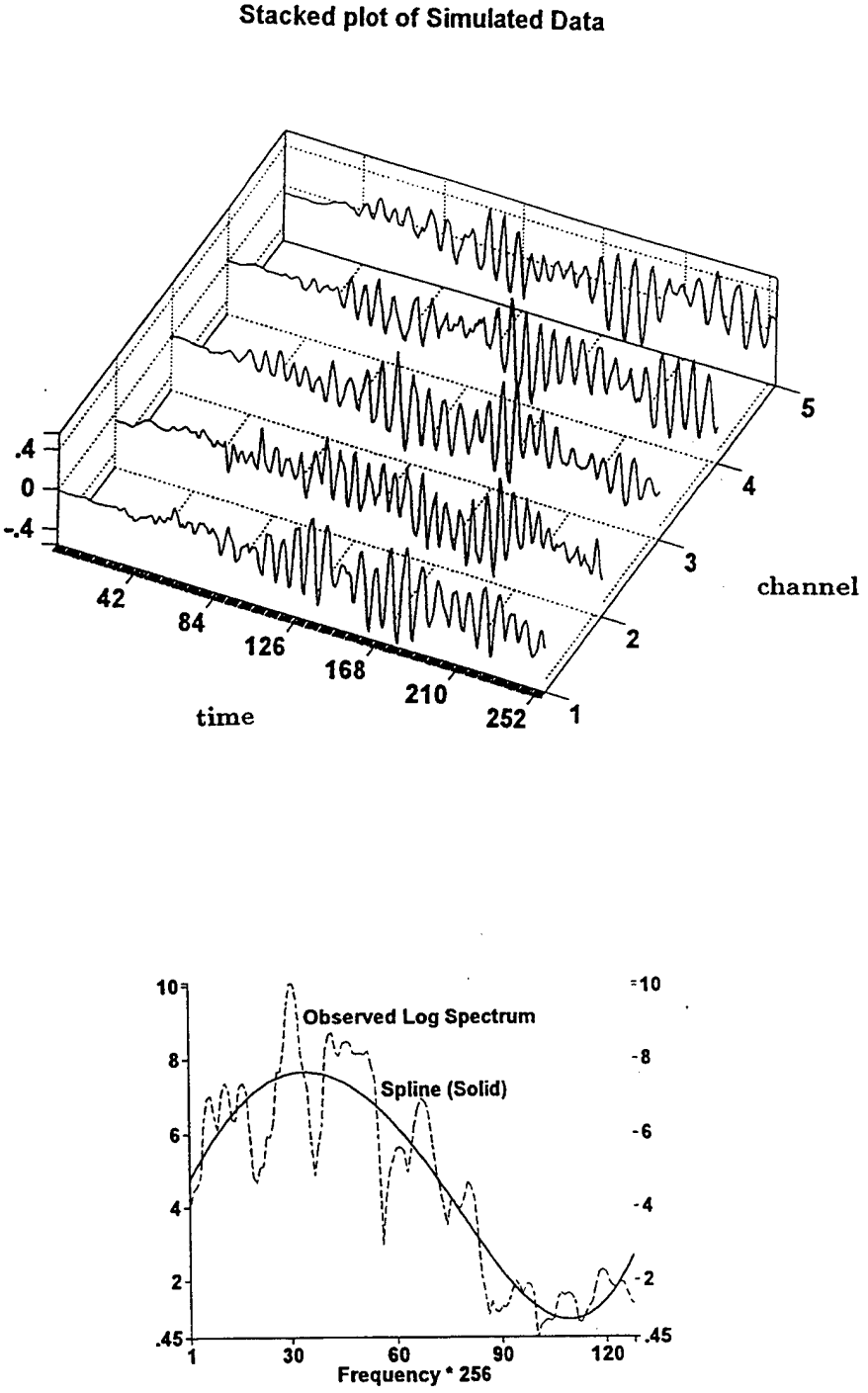

Figure 2: A Contrived Array With Delay Firing (d=8,15,23,30) and the Associated Detrended Log Spline Spectra.

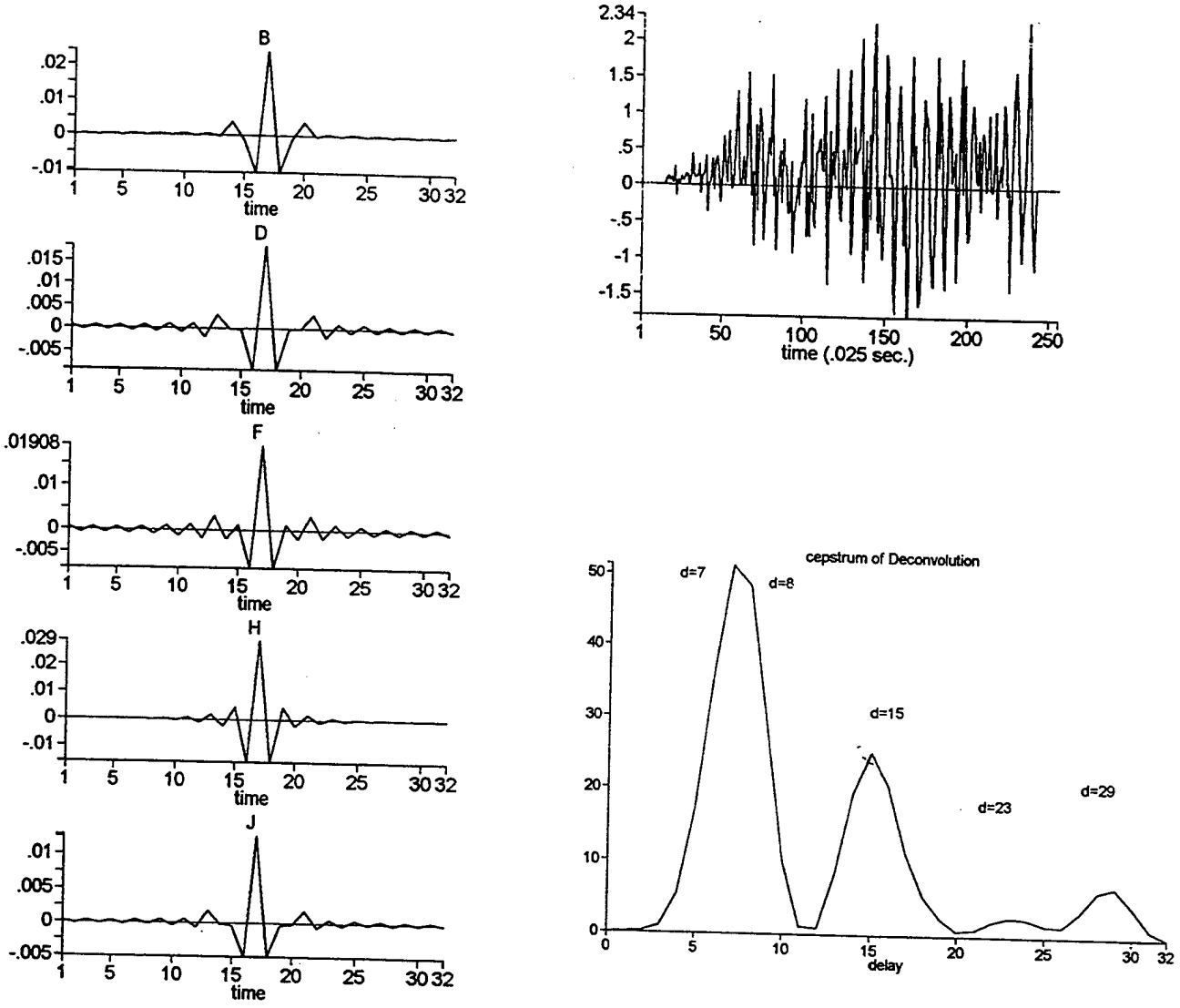

Figure 3: The Bank of Deconvolution Filters (Left) With Deconvolved Signal (Top Right) and Cepstrum of Deconvolved Signal (Bottom Right)

it appears to be the sum of a smooth trend component, $\log|A_j(\nu)|^2$, fitted as a cubic spline with a single knot at 0.25 cycles per point, and a periodic component, corresponding to $\log|\theta(\nu)|^2$.

Figure 3 shows the bank of deconvolution filters $h_j(t), j = 1, \ldots, 5$ in the left panel and the resulting deconvolved signal $\hat{x}(t)$ in (4). To find the cepstrum of the deconvolved signal, take the discrete Fourier transform

$$\hat{X}(\ell) = T^{-1/2} \sum_{t=0}^{T-1} \hat{x}(t) \exp\{-2\pi i \ell t/T\} \tag{11}$$

of the deconvolved series and compute the spectrum of the log periodogram as

$$C(d) = T^{-1/2} \sum_{\ell=0}^{T/2-1} \log|\hat{X}(\ell)|^2 \exp\{2\pi i \ell d/T\}, \tag{12}$$

expressed as a function of delay, d, in points. The cepstrum of the deconvolution, shown in the bottom right panel of Figure 3, isolates delays at $\tau = 7, 8, 15, 23$, and 29 points. From the nature of the contrived data, we expect delays at $7, 8, 15, 16, 23$, and 31 points with potentially the strongest components corresponding to time delays of 7 or 8, appearing four times, 15 or 16, which appear three times, 23 points which appears twice and 31 points which appears once.

3. Seasonal Multiplicative ARMA Models for Arrays

There is a form of (3) that fits into the multiplicative seasonal ARMA developed by Box and Jenkins (see Box, Jenkins and Reinsel, 1994). For this case we let $x(t)$ in (1) be defined for time delays $\tau_k = kd, k = 1, 2, \ldots, n$ that are multiples of some underlying assumed firing delay d, so that one might envision a multiplicative model, driven by white noise processes $w_j(t)$, of the form

$$y_j(t) = \frac{\Theta(B^d)}{\phi(B)} w_j(t) \tag{13}$$

for the output, where B denotes the delay operator, i.e. $B^k x(t) = x(t-k)$, so that the n reflections at multiples of d are expressed by the polynomial operator

$$\Theta(B^d) = \sum_{k=0}^{n} \theta_k B^{kd} \tag{14}$$

with $\theta_0 = 1$. The autoregressive operator of order p,

$$\phi(B) = \sum_{k=1}^{p} \phi_k B^k, \tag{15}$$

defines the input signal. Dargahi-Noubary (1995) has argued that many seismic source function models can be regarded as having been generated by the one-parameter third-order autoregressive model (p=3), with

$$\phi(B) = (1 - e^{-k_0} B)^3 \tag{16}$$

where k_0 is an unknown parameter. Combining (13) and (16) leads to a seasonal ARMA with a third order autoregressive component and a d^{th} order moving average component with period n that can be written as

$$y_j(t) - 3e^{-k_0} y_j(t-1) + 3e^{-2k_0} y_j(t-2) - e^{-3k_0} y_j(t-3) = w_j(t) + \sum_{k=1}^{n} \theta_k w_j(t - kd). \tag{17}$$

In the above model, the delay d corresponds to the spacing of the charges in the ripple fired event and the number of pulses n might be proportional to the number of shots. Hence, the model selected will depend on both d and n, whereas the parameters estimated under each model are $k_0, \theta_1, \theta_2, \ldots, \theta_n$ and the variance of $w_j(t)$, say σ_w^2, assuming a common variance for the stochastic inputs generating the signal. The underlying time domain model is more specific in specifying the duration or seasonal increment and in assuming that the smooth component of the spectrum is generated by a single-parameter third-order autoregressive model. Note that the general third-order model has also been proposed by Tjøstheim (1975) as a model for short period seismic data.

Minimizing the sum of squared errors for specified values of n and d leads to the objective function

$$SSE(k_0, \theta_1, \theta_2, \ldots, \theta_n) = \sum_{j=1}^{N} \sum_{t=nd}^{T} w_j^2(t), \tag{18}$$

which maximizes the log likelihood, and we may estimate σ^2 as

$$\hat{\sigma}^2 = \frac{1}{NT'} \sum_{j} \sum_{t} \hat{w}_j^2(t), \tag{19}$$

where the nonlinear optimization only involves $NT' = N(T - nd + 1)$ residuals. In order to select a model, we choose n and d as the joint minimizers of the *Bayesian Information Criterion (BIC)* of Schwarz, 1978, say

$$BIC(n, d) = \log \hat{\sigma}^2 + \frac{(n+1)\log(NT')}{NT'}. \tag{20}$$

The Schwarz criterion is consistent, i.e., the probability of fitting the wrong order model converges to zero, whereas procedures based on *Akaike's Information Theory Criterion (AIC)* (Akaike, 1973), are not and lead to overfitting in some cases. If one has the idea that there exists a true model of some order and the sample is quite large, as in the present situation, it is more reasonable to use the Schwarz criterion. If one is inclined to think of finding the best approximation to some unknown model of possibly infinite order, the various AIC measures are asymptotically efficient (Shibata, 1980) whereas BIC is not. For a summary of the nonlinear Gauss-Newton estimation procedure applied to the repeated measures ARMA model, see Shumway(1988).

To give an example, consider searching the contrived data in Figure 2 for the best fitting seasonal ARMA process. It is convenient to limit the number of reflections to the possible range $1 \leq n \leq 6$ and the delays to the range $4 \leq d \leq 13$. We begin with $d = 4$, so as not to confuse the delays with the first three lags of the autoregressive part. Figure 4 shows the resulting values of BIC and we note that there are a number of local minima, mostly occurring at $d = 8$. The global minimum, however, is attained for $n = 4, d = 4$, and would lead to values that differ from the correct values $n = 4, d = 8$. The estimates $\hat{\theta}_j, j = 1, 4$ in this latter case were $-.47, .58, -.60, .16$ and the alternating signs are not reasonable for the application. The most reasonable model, for $n = 3, d = 8$ had the third smallest BIC and gave positive estimates $(.83, .41, .15)$ for the parameters and $\hat{k}_0 = .98$. The ambiguity in the multiple local minima, largely due to the difficulty of estimating the number of reflections n, suggests looking at values of BIC averaged over n, shown in the lower panel of Figure 4. The consistency of the minima for $d = 8$ suggests taking this value, which turns out to be reasonable from the individual time delays, placed at $\tau_1 = 8, \tau_2 = 15, \tau_3 = 23, \tau_4 = 31$ points respectively with weights $\theta_1 = .9, \theta_2 = .9, \theta_3 = .6, \theta_4 = .7$. In summary, there are more possible interpretations for the ultimate model implied by the time domain analysis and few approximate statistical significance tests are available for the number of reflections. One might consider testing against a model with $n = 0$, but we did not do so because of the number of possible alternatives.

Stacked Plot of BIC for Simulated Data

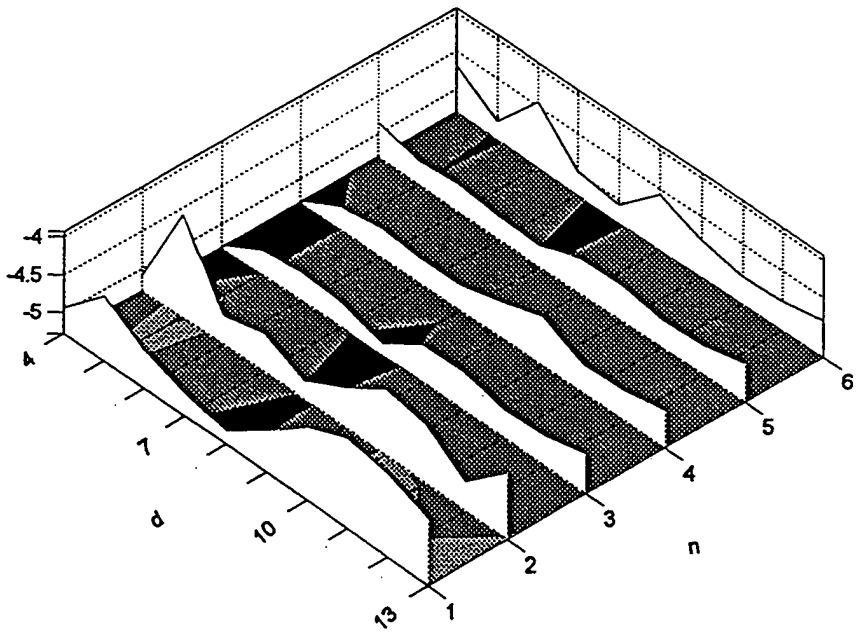

Stacked Plot of Average BIC for Simulated Data

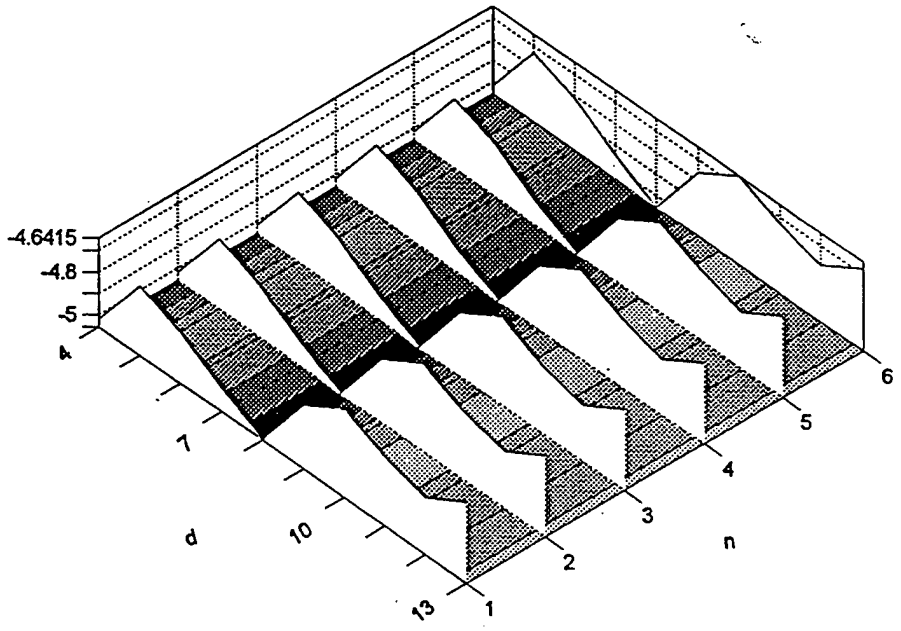

Figure 4: BIC Contours for Seasonal ARMA Search Using Contrived Data. The darkest value corresponds to the minimum. The bottom panel averages BIC over the number of reflections and shows a consistent delay at $d = 8$ points.

4. The Nonlinear Cepstral F Detector

We may also take a nonlinear approach based on the multiplicative model (2). Note that the spectrum of the observed series $y_j(t)$ in this case has the representation

$$\begin{aligned} P_{y_j}(\nu) &= |A_j(\nu)|^2 P_x(\nu) P_{n_j}(\nu) \\ &= |A_j(\nu)|^2 |\theta(\nu)|^2 P_s(\nu) P_{n_j}(\nu), \end{aligned}$$

using (6). Then, taking logarithms yields the additive decomposition

$$\log P_{y_j}(\nu) = \log |A_j(\nu)|^2 + \log |\theta(\nu)|^2 + \log P_s(\nu) + \log P_{n_j}(\nu)$$

To follow up on the suggestion in Section 2, based on the additive decomposition above, we consider computing the logarithm of the spectral estimator at each channel. Defining the discrete Fourier transform of $y_j(t)$ as $Y_j(\ell)$ (see (11)) at frequencies $\nu_\ell = \ell/T, \ell = 0, 1, \ldots, T/2 - 1$, we have the representation

$$\log |Y_j(\ell)|^2 = \log P_s(\nu_\ell) + \log |A_j(\nu_\ell)|^2 + \log |\theta(\nu_\ell)|^2 + \log |N_j(\ell)|^2, \qquad (21)$$

where $|N_j(\ell)|^2$ is the periodogram, known to have approximately a chi-squared distribution with 2 degrees of freedom when the noise $n_j(t)$, for example, is a linear process (see Hannan, 1971, p. 249). Subject to regularity conditions on the linear process, the variance is proportional to to the square of the spectrum, with an error term that is $O(T^{-1})$. Furthermore, for two frequencies separated by multiples of $1/T$, the correlation is of the same order. Since the variance is proportional to the square of the mean, we may expect the logarithm to have an approximately constant variance. If one smoothes the periodogram at all, say over L adjacent frequencies (L=3 for the examples in this paper), the distribution of the logarithm of the smoothed spectrum will be close to a normal distribution. This suggests that, as an approximation, the error series in (21) could be regarded as stationary normal processes.

BHT (1962) also suggested that, in the case of a single series, the log spectrum, as a function of frequency, might be regarded as a pseudo-time series and that the *cepstrum* be used to identify the periodicities (time delay differences) in the same way that the spectrum does for conventional time series. In accordance with previous arguments, it is clear that $|\theta(\nu_\ell)|^2$ will have periods equal to $T/(\tau_j - \tau_k)$ and so the logarithm of the periodogram will tend to a general shape having peaks at $(\tau_j - \tau_k)/T, j, k = 1, \ldots, n$. Overall, it is clear that the logarithm of the periodogram of the observed series in (21) will still be nonstationary because of the likelihood that the component $\log |A_j(\nu_\ell)|^2$ will vary substantially over frequency and in a manner that changes for different recording instruments.

Since the raw series is also expected to have a nonstationary mean component, one could detrend, subtracting a reasonable estimate of the smooth function upon which the approximately stationary series rides. Any relatively smooth detrending will work; the method used here was to fit a cubic spline with a single knot in the middle of the record under the assumption that the underlying nonstationary component of the spectrum is very smooth with a slight inflection point about half way through the record. Moving average smoothing, called *liftering* by BHT, will also work but the length required subjects the series to serious end effects. Once the detrending has been done, we work with the resulting series and do not make further use of the functional form of the spline. Here, we envision the component $\log|A_j(\nu)|^2 + \log P_s(\nu)$ as a relatively smooth function that can be approximated by a cubic spline with one knot as in (10). We estimate the parameters and consider the *detrended* log-periodogram model

$$\log \frac{|Y_j(\ell)|^2}{|A_j(\nu_\ell)|^2 P_s(\nu_\ell)} = \log|\theta(\nu_\ell)|^2 + \log|N_j(\ell)|^2. \tag{22}$$

The detrended log-periodogram is expressed in terms of a common signal $\log|\theta(\nu_\ell)|^2$ and a noise term $\log|N_j(\ell)|^2$ which differs from site to site and represents local site effects.

To illustrate some of the above ideas, consider again the simulated ensemble of signals shown in the top panel of Figure 2. The five resulting series, shown in Figure 2, all contain slightly different signals at the same set of delays and we can argue that the model given above is plausible and that any method based on the model should work reasonably well. A typical observed spectrum is shown in the bottom panel of Figure 2 and we note that it appears to be the sum of a smooth trend component, $\log|A_j(\nu)|^2 + \log P_s(\nu)$, shown as a solid line, a periodic component, corresponding to $\log|\theta(\nu)|^2$ and a departure from the periodic component corresponding to $\log|N_j(\nu)|^2$. The observed log spectrum is nonstationary because of the smooth component and, as suggested earlier, it would be natural to detrend the log spectrum to eliminate the effect of the smooth function $\log|A_j(\nu)|^2 + \log P_s(\nu)$. The left panel of Figure 5 shows the result of this adjustment at each channel as dotted lines and it is clear that one might regard the detrended result as the sum of a periodic function and noise, as in the periodogram model given above. Furthermore, the average of the log spectra might be regarded as an estimator for $\log|\theta(\nu)|^2$ and we show the average in Figure 5 as a solid line superimposed on the five separate detrended log spectra. The average seems to enhance the underlying periodic signal and we suggest later that the deviation from these overall means are basically estimators for the log spectra of the noise processes, $\log f_j^n(\nu)$. The result of detrending with a cubic spline, as depicted in the lower panel of Figure 2, has the appearance of a stationary signal

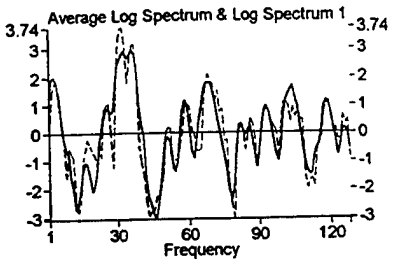

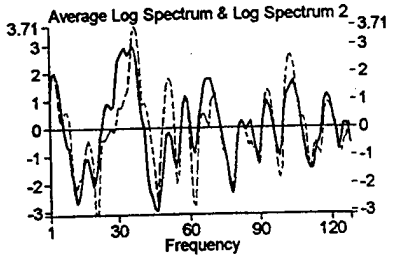

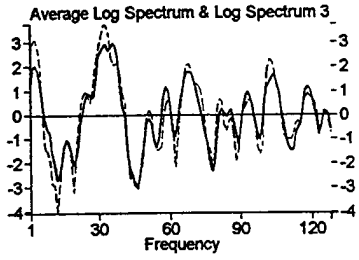

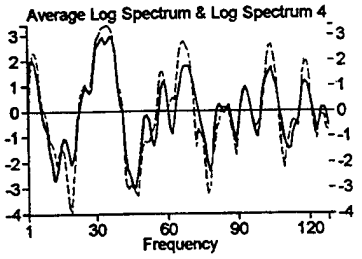

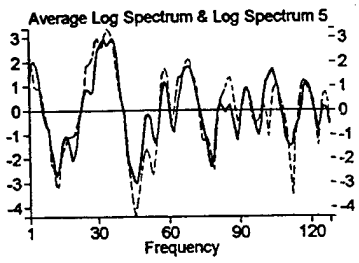

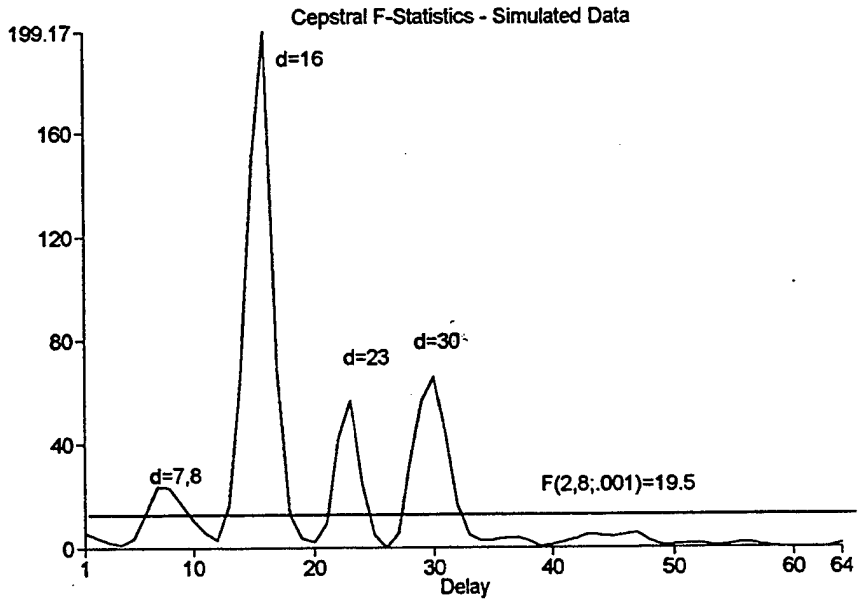

Figure 5: Bank of Detrended Log Spectra (Right) and the Cepstral F-Statistic Showing Peaks at 8, 16, 23 and 30 points.

with several periodic components corresponding to the time delay differences previously mentioned. Here, we might expect periodicities at $\tau_j - \tau_k = 7, 8, 15, 16, 23, 31$, with potentially the strongest components corresponding to time delays of 7 or 8 points, which appear four times, time delays of 15 or 16 points, which appear three times, a time delay of 23 points, which appears twice and a time delay of 31 points, which appears once.

This example and model (22) above motivates an approach to detecting a common signal on an array that is similar to that given in Shumway (1971), where the discrete Fourier transform, say

$$Q_j(d) = T^{-1/2} \sum_{\ell=0}^{T/2-1} \log \frac{|Y_j(\ell)|^2}{|A_j(\nu_\ell)|^2 P_s(\nu_\ell)} \exp\{2\pi i \ell d/T\}$$

is regarded as behaving like the transform of a stationary process in the delay $d = 0, 1, \ldots, T/4$ at each channel so that one may write the signal plus noise model

$$Q_j(d) = S(d) + V_j(d), \tag{23}$$

where the right hand side contains the transforms of the right hand side of (22). Here, the signal transform $S(d)$ is fixed and unknown and the noise $V_j(d)$ has approximately a complex Gaussian distribution with mean 0 and variance $\sigma^2(d)$ at delay d. The Fourier transform of such a process will be in the form of a sum of constants multiplied by adjacent values of the approximately normally distributed log periodogram or smoothed spectra. The linear combination will be approximately normal, since the components are approximately normal, and will tend toward normality by central limit arguments even when the components are not that close to normality. The noises are assumed uncorrelated for different j and have identical cepstra, $\sigma^2(d)$, at each channel. This was checked for several events and found to be reasonable.

Then, motivated by the classical approach to detecting a signal in N stationarily correlated time series, we note that testing the hypothesis $S(d) = 0$ leads to an F-Statistic involving the total stacked cepstra (SCT)

$$SCT(d) = \sum_{j=1}^{N} |Q_j(d)|^2 \tag{24}$$

and the spectrum of the stacked log spectra or mean stacked cepstra (SCM), say

$$SCM(d) = N|\bar{Q}(d)|^2, \tag{25}$$

where

$$\bar{Q}(d) = N^{-1} \sum_{j=1}^{N} Q_j(d) \tag{26}$$

is the mean Fourier transform of the array log-spectra. Figure 5 shows the original detrended log-spectra with the mean of the array log-spectra superimposed on each series and we note that the common periodicities are enhanced in the stack. An important quantity involved in the optimal detection statistic is the error cepstrum (SCE), defined as

$$\begin{aligned} SCE(d) &= \sum_{j=1}^{N} |Q_j(d) - \bar{Q}(d)|^2 \\ &= SCT(d) - SCM(d), \end{aligned} \tag{27}$$

which is a measure of the extent to which the individual channel transforms differ from the mean transform. It can be interpreted as the *cepstral noise* component. The F-Statistic resulting from the signal detection hypothesis is given by

$$F_{2,2(N-1)}(d) = (N-1)\frac{SCM(d)}{SCE(d)} \tag{28}$$

and can also be interpreted as a cepstral *signal to noise ratio.* The subscripts refer to an F distribution with 2 and $2(N-1)$ degrees of freedom. Note that the total cepstrum (24) is exactly the *sum-stack* proposed by Alexander et al (1995), computed by adding up the separate cepstra. Alexander et al have also considered the product-stack which does not appear to have any identifiable statistical properties and we do not analyze it here. It is clear that the sum-stack will not reflect the common signal components as well as either the cepstral component due to the signal or the F-Statistic (28).

To illustrate, we return again to the contrived data shown in Figure 2 which contains signals with a known configuration of delays. The average of the log spectra, shown in the left panel of Figure 5, is an approximately unbiased estimator of $\log|\theta(\nu_\ell)|^2$ in (22); its transform estimates $S(d)$ in (23). Figure 5 shows the F-Statistic corresponding to the contrived data shown in Figure 2. Note the strong components appearing at delays of 8, 15, 23, 30, and 36 points that may be compared with the known true delays 8, 15, 23, and 31 points. Note that the true time delays would imply frequencies of the form 7, 8, 15, 16, 23, and 31 points respectively. The cepstral F-Statistic, shown in the right panel of Figure 5, provides a statistical level of significance for the various peaks and we note that the significant peaks are 8, 16, 23, and 30 points so that the smallest of the larger peaks at d=36 in the stacked cepstrum is not significant. All peaks are significant at a false alarm

rate of .001. In general, since there are often a large number of delays of interest, one should insist on at least .01 as a level of significance.

5. Analysis of Kola Mining Explosions

For testing on actual data, we focussed on the deonvolution and cepstral F methodologies. The parametric seasonal ARMA models of Section 3 were often unstable and it was difficult to obtain reasonable estimators for the weights $\theta_1, \theta_2, \ldots, \theta_n$ for the simulated data. In addition, the estimation procedure seemed to be unduly sensitive to restricting time delays to be constant multiples of some underlying delay d. In contrast, the nonparametric deconvolution and cepstral F methods concentrated on isolating only time delay differences on the theory that a consistent set of time delay differences will produce a strong peak in the cepstrum of the deconvolved signal or in the cepstral F-Statistic. This was more in line with the idea that time delays induced in ripple-firing may be somewhat irregular. For the simulated data, both frequency domain methods isolated the predictable time delay differences.

Data used for testing the frequency domain methodology were from mining explosions in the Kola Peninsula, situated in the Russian Arctic. Ten mining explosions at the HD9 quarry were observed at 5 channels of the ARCESS Array in northern Norway (see Der et al, 1987). Figure 1 shows at typical mine blast (110), sampled at .025 seconds, and we note that the four phases P_n, P_g, S_n, and L_g are fairly obvious. This is typical of the other events (054, 066, 138, 147, 182, 219, 246, 282, and 285) and it was fairly easy to construct four files containing the separate phases for each of the 10 events. Figure 1 shows, in the bottom panel, the five series used for the P_n phase of event 110.

The quantities of interest will be the cepstrum of the deconvolved signal $\hat{x}(t)$, given by (11) and (12) for method (i), and the cepstral F-Statistic (28) for method (iii). Figures A1-A20 show plots of the two statistics for each of the 10 events (four phases per plot). We used 256 point samples for all phases except L_g, which had 512 points. Ripple-firing may be indicated best by a consistent pattern of strong peaks, with delay time differences within the time intervals that might be plausible for delays or their aliases. Sampling is 40 points per second and the delays are given in points. To convert to milliseconds (ms) multiply by 25. For example, Figure A1 shows peaks at 4, 10-11, 16, 21, and 26, which might imply a ripple delay of 5-6 points or of 125-150 ms. Unfortunately, Figure A2, which plots the F-Statistic does not confirm a consistent delay in that range. Note that the significance values for the F-Statistic at the levels .001, .01, and .05 for 2 and 8 degrees of freedom are 18.5, 8.7, and 4.5, respectively.

Table 1: Delays (in pts.) for Deconvolved Cepstra and Cepstral F Statistics

Event	Phase			
	P_n	P_g	S_n	L_g
	Deconvolutions			
054	4,14,21,29	5,12,21,26	4,11,16,21,26	5,15,28
066	2,10,23,29	3,10,17,22	8,14,20,28	4,14
110	2,23	7,17	8,14,21,29	3,9,18,25
138	3,9,14,23	4,10,22,28	4,11,31	6,18,24,30
147	3,8,14,20,24,29	6,17,21,26	6,11,16,31	3,7,11,15,20,29
182	4,14,21	5,10	7,19,26	5,13,19,25
219	3,9,15,28	2,8,11,15,22	6,11,19	3,7,11,15,23
246	3,8,13,18,27	5,10,17,26	3,7,11,20	4,11,18,24
282	6,12,22	2,15,20,25	3,9,15,19,26	2,11,16,26
	Cepstral F			
.5in				
054	4,21	2,11,20	2,12,21	3
066	11,23	11,15,22,30	2,12	
110	7,14,24	8,25	12	2,9,21,25
138	2,8,18,31	11,22,30	2,12,19,26	2,10,18,24
147	7,20	7,31	2,7,14,21,28	2,7,15,24
182	4,21	3,17,30	8,13,20,28	8,13,18,22,25
219	4,15,20,25,30	6,15,26	10,19,25	8,11,16,23
246	12,23	6,10,24,30	7,13	10,19,22
282	11,21,25,31	14,22,29	12,19,24,30	3,11,16
285	3,11,17,22,26	3,11,17,26	5,13,18,27	7,18

We went through all the plots and extracted what appeared to be the most significant peaks in the time delays for both the cepstra of the deconvolved series and the cepstral F-Statistic. That information is given in Table 1. The results overall are somewhat disappointing. There is less consistency between the two measures than one would have expected, with the F-Statistic generally yielding fewer significant peaks. For example, Figure A8, for Event 138, shows evidence of weak rippling (.01 and .05 levels) in the P_n and S_n and L_g phases but not in P_g. Figure A7 from the same event shows rippling in the P_n and S_n phases but not really in the other two phases. One might possibly identify consistent rippling at time delays from 6-10 points, i.e. 150-250 ms for this particular event. Other

events are roughly similar, with the evidence of delay firing often indicated weakly in the range 125-250 ms.

It is clear from Table 1 that all phases tend to show evidence of delays for various events but that there are no clear indications that the same patterns for all phases and both statistics hold for any event in this data set. Given the successes enjoyed by both methods on simulated data, one would have to say that the evidence for consistent ripple firing over all phases in the Kola mining data is rather weak. In addition, there is not a single phase that seems to do well for all events. Of course, a larger array, say of 30-40 elements, could be helpful for greater enhancement of the common pattern and cancellation of patterns that are due to local reverberations.

6. Discussion

In this project, we have developed and tested three methods for detecting ripple-firing on arrays. In simulations, it is clear that the two methods based on the cepstrum, i.e., cepstral analysis of the deconvolved signal and the cepstral F-Statistic offer the most promise. We prefer the cepstral F-Statistic for the following reasons.

1. The two quantities involved in the cepstral F are comparable to those appearing in the cepstral stack proposed by Alexander et al (1995) for the purpose of estimating P-pP reflection delays. Hence, the computed statistic is a function of quantities that are accepted as meaningful in the seismic literature.

2. The statistic has a convenient interpretation as a signal to noise ratio and a known statistical distribution under the hypothesis of no delay firing. Hence, we can set a specific level for false alarms. These statistical properties distinguish its performance from that of the simple stacked spectra of Alexander et al (1995).

3. Since the underlying model is for the squared periodogram, it is not critical to line the signals up on the array. That is, the form is related to incoherent beam forming.

It would be remiss not to mention that Alexander et al (1995) primarily apply their methods to the problem of determining source depth. This is functionally related to the distance between the primary P wave and the single reflection pP. This problem is somewhat easier since there is conceptually only one reflection and we would have $n = 1$ in (7), i.e.

$$|\theta(\nu)|^2 = 1 + \theta_1^2 + 2\theta_1 \cos(2\pi\nu d)$$

with only a single frequency to detect. Hence, it would be interesting to apply the cepstral F-Statistic to the depth determination problem as an alternative to the simple sum and product stacks employed by Alexander et al (1995).

7. References

Akaike, H. (1973). Information theory and an extension of the maximum likelihood principle. In B.N. Petrov and F. Csáki ed. *2nd International Symposium on Information theory*, 267- 281, Budapest: Akadémia Kiadó.

Alexander, S.S., R.C. Hsu, S.L. Karl, I.N. Gupta and D.H. Salzberg (1995). New techniques for estimating source depth and other diagnostic source characteristics of shallow events from regional observations of P, Lg and Rg Signals, Report No. PL-TR-95-2108, Phillips Laboratory, Directorate of Geophysics, Air Force Materiel Command, Hanscom AFB, MA 01731-3010. ADA 310037.

Baumgardt, D.R. and K.A. Ziegler (1988). Spectral evidence for source multiplicity in explosions: Application to regional discrimination of earthquakes and explosions. *Bull. Seismolog. Soc. of Amer.*, **78**, 1773-1795.

Bogert, B.P., M.J.R. Healy and J.W. Tukey (1962). The frequency analysis of time series for echoes: cepstrum, pseudo-autocovariance, cross cepstrum and saphe cracking. In *Proceedings of a Symposium on Time series Analysis*, ed. M. Rosenblatt. New York: John Wiley.

Box, G.E.P., G.M. Jenkins and G.C. Reinsel (1994). *Time Series Analysis, forecasting, and Control*, 3rd ed., Prentice Hall, Englewood Cliffs, New Jersey.

Chapman, M.C., G.A. Bollinger and M.S. Sibol (1992). Modeling delay-fired explosion spectra and source function deconvolution at regional distances. Final Report No. PL-TR-92-2250, Phillips Laboratory, Directorate of Geophysics, Air Force Materiel Command, Hanscom Air Force Base, MA 01731-5000, ADA260232.

Dargahi-Noubary, G.R. (1995). Stochastic modeling and identification of seismic records based on established deterministic formulations. *J. Time Series Analysis*, **16**, 201-219.

Der, Z.A., Shumway, R.H. and Lees, A.C.(1987). Multi-channel deconvolution of P waves at seismic arrays. *Bull. Seismolog. Soc. Amer.*, **77**, 195-211.

Der, Z.A., A.C. Lees, K.L. McLaughlin and R.H. Shumway (1992). Multichannel deconvolution of short period teleseismic and regional time series. Chapter 9 in *Statistics in the Environmental and Earth Sciences*, A.T. Walden and P. Guttorp (eds.), 156-188. London: Edward Arnold (New York: Halsted Press).

Der, Z.A., D.R. Baumgardt and R.H. Shumway (1993). The nature of particle motion in regional seismograms and its utilization for phase identification. *Geophy. J. Int.*, **115**,

1012-1024.

Hannan, E.J. (1970). *Multiple Time Series.* New York: Wiley.

Hannan, E.J. and P.J. Thomson (1974). Estimating echo times. *Technometrics*, **16**, 77-84.

Hedlin, M.A.H., J.B. Minster and J.A. Orcutt (1990). An automatic means to discriminate between earthquakes and quarry blasts. *Bull. Seismolog. Soc. Amer*, **80**, 2143-2160.

Schwarz, G. (1978). Estimating the dimension of a model. *Ann. Statist.*, **6**, 461-464.

Shibata, R. (1980). Asymptotically efficient selection of the order of the model for estimaing parameters of a linear process. *Ann. Statist.*, **8**, 147-164.

Shumway, R.H.(1971). On detecting a signal in N stationarily correlated noise series. *Technometrics*, **10**, 523-534.

Shumway, R.H. and R.R. Blandford (1978). On detecting and estimating multiple arrivals from underground nuclear explosions. *SDAC-TR-77-8*, Seismic Data Analysis Center, Teledyne Geotech, 314 Montgomery St., Alexandria, VA 22314, Sponsored by the Defense Advanced Research Projects Agency.

Shumway, R.H. (1988). *Applied Statistical Time Series Analysis.* Englewood Cliffs, New Jersey: Prentice Hall.

Shumway, R.H. and Der, Z.A.(1985). Deconvolution of multiple time series. *Technometrics*, **27**, 385-393.

Shumway, R.H., D.R. Baumgardt and Z.A. Der (1998). A cepstral F-statistic for detecting delay-fired seismic signals. *Technometrics*, **40**, 100-110.

Tjøstheim, D. (1975). Some autoregressive models for short-period seismic noise. *Bull. of Seism. Soc. Amer.*, **65**, 677-691.

Appendix A:

Cepstral Analyses of Kola Peninsula Events

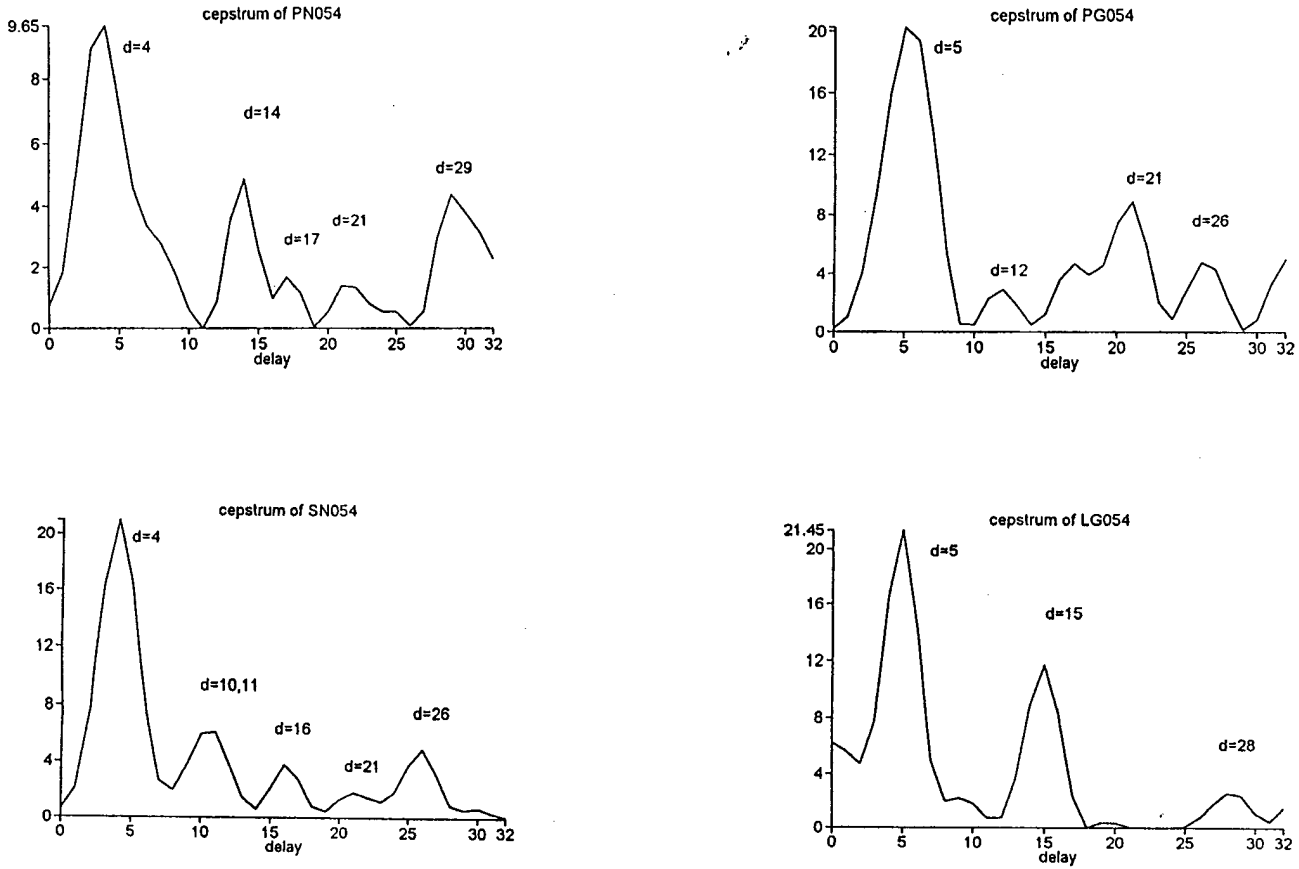

Figure A1: Cepstral Analysis of Deconvolved Array Signal for Four Phases From Event 054 (Delay in points).

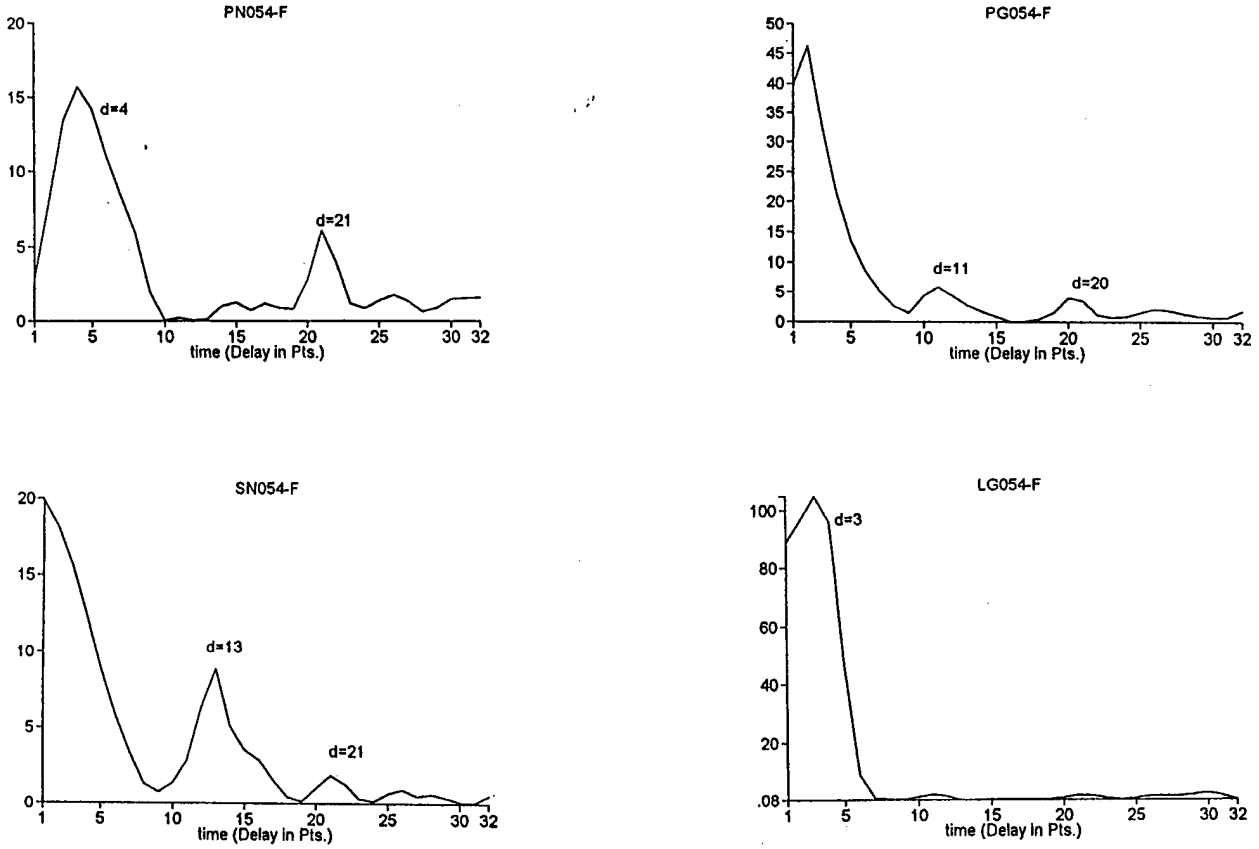

Figure A2: Cepstral F-Statistic for Four Phases From Event 054 (Delay in points).

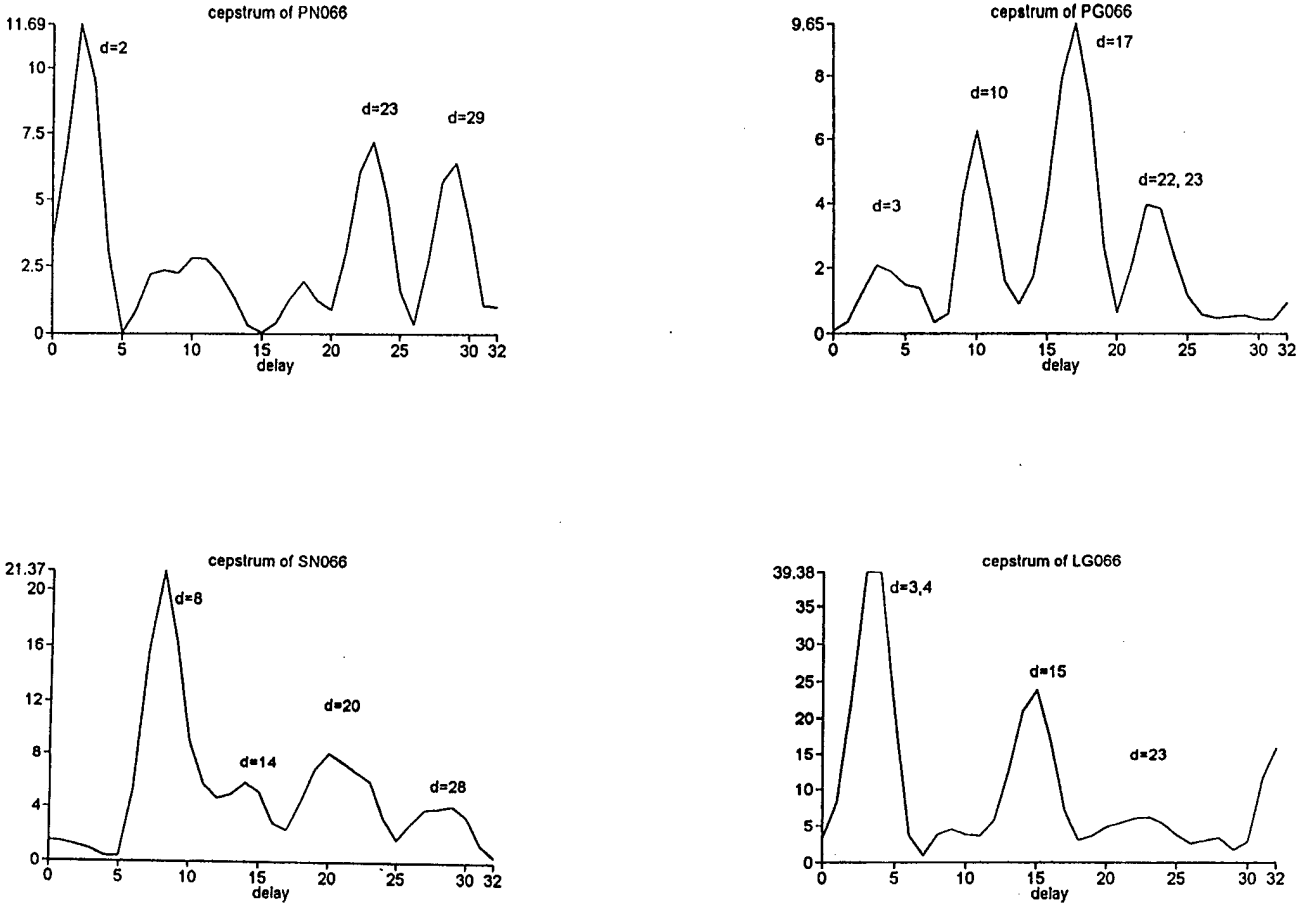

Figure A3: Cepstral Analysis of Deconvolved Array Signal for Four Phases From Event 066 (Delay in points).

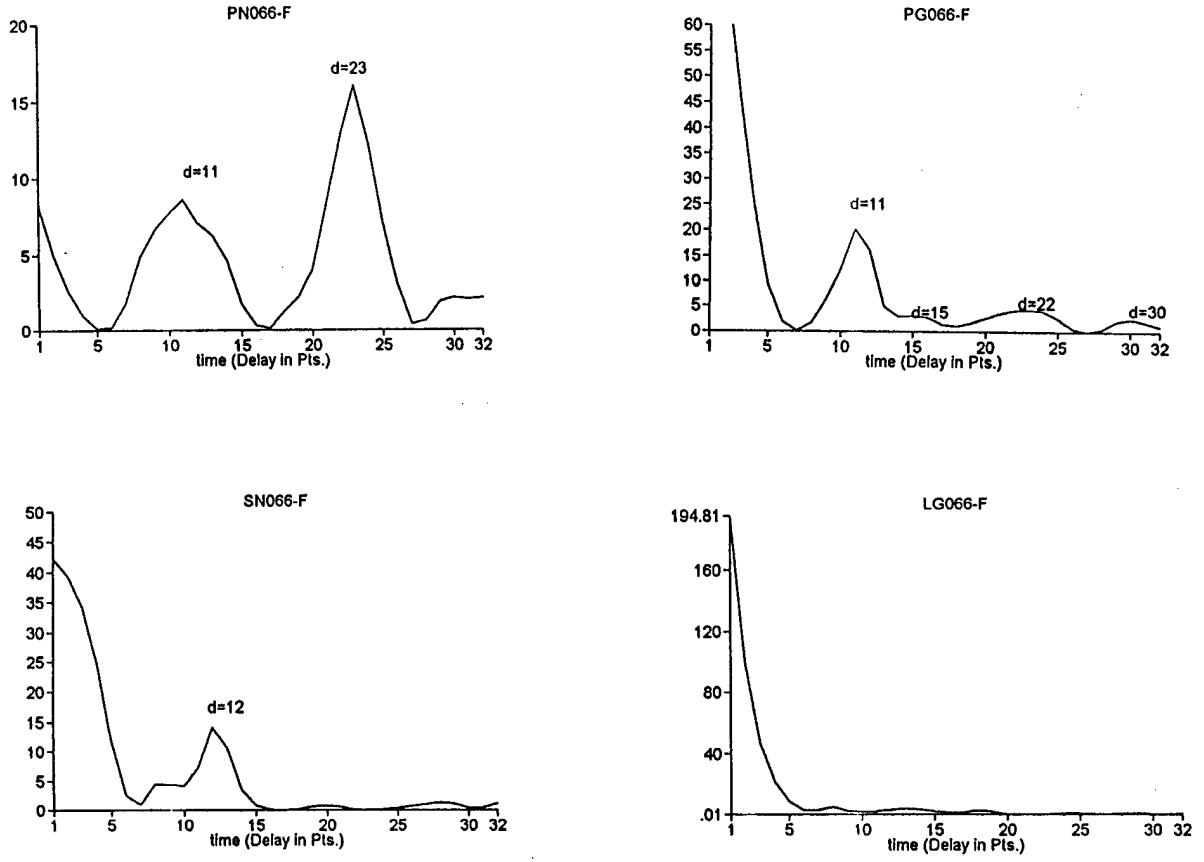

Figure A4: Cepstral F-Statistic for Four Phases From Event 066 (Delay in points).

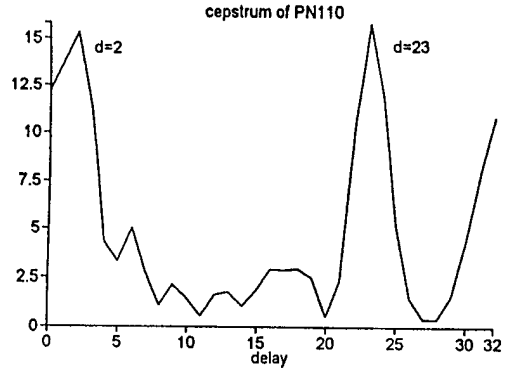

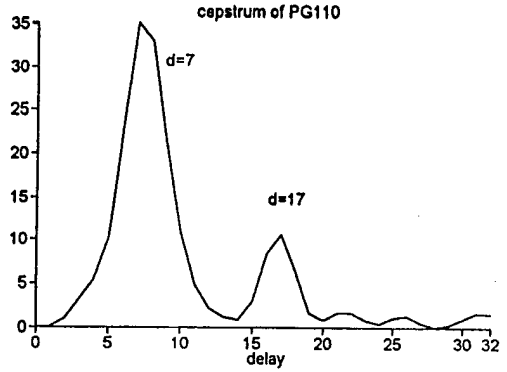

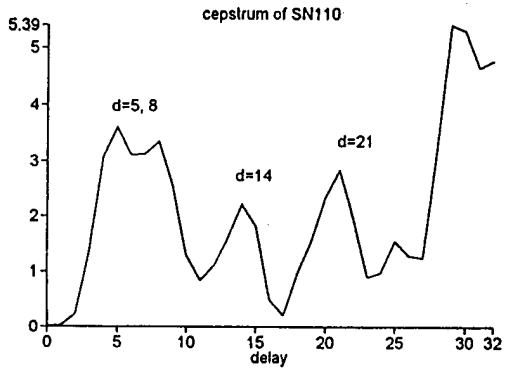

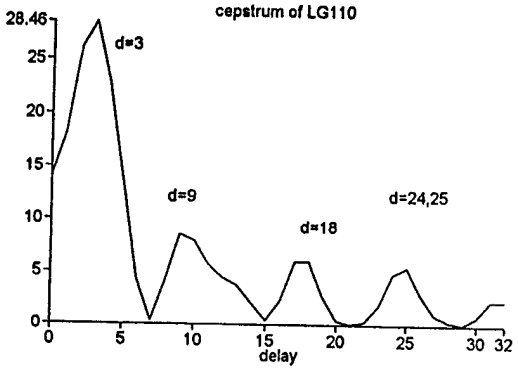

Figure A5: Cepstral Analysis of Deconvolved Array Signal for Four Phases From Event 110 (Delay in points).

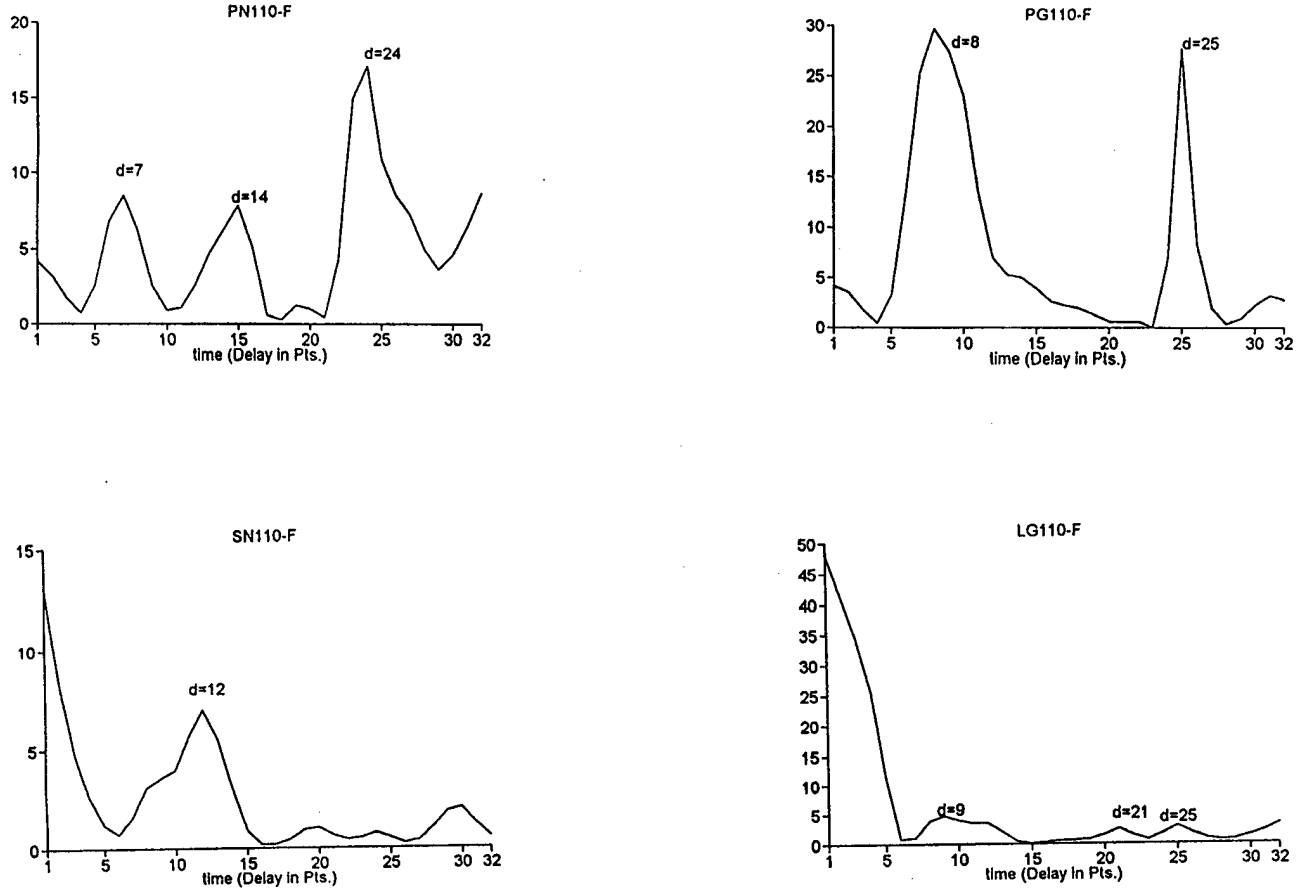

Figure A6: Cepstral F-Statistic for Four Phases From Event 110 (Delay in points).

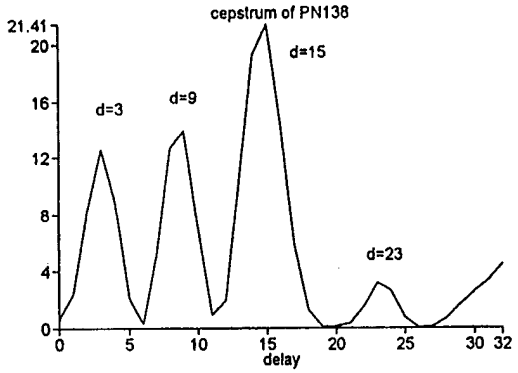

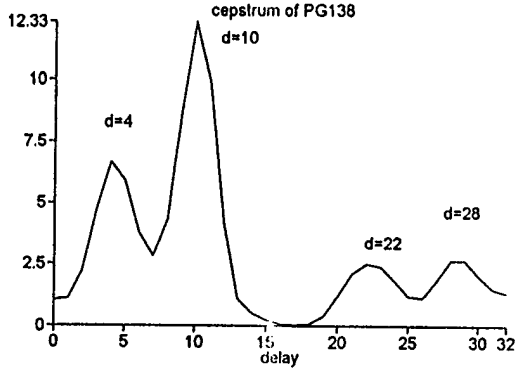

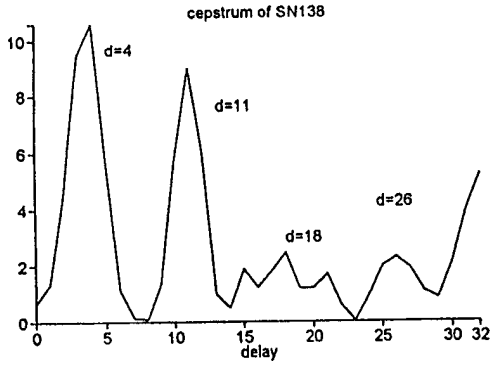

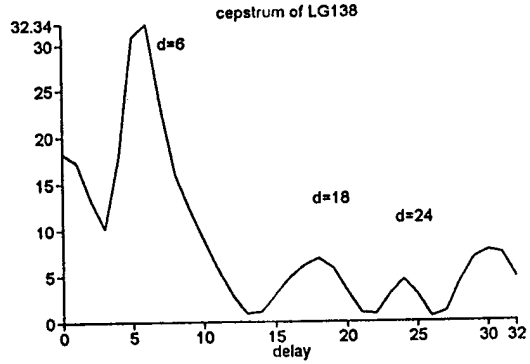

Figure A7: Cepstral Analysis of Deconvolved Array Signal for Four Phases From Event 138 (Delay in points).

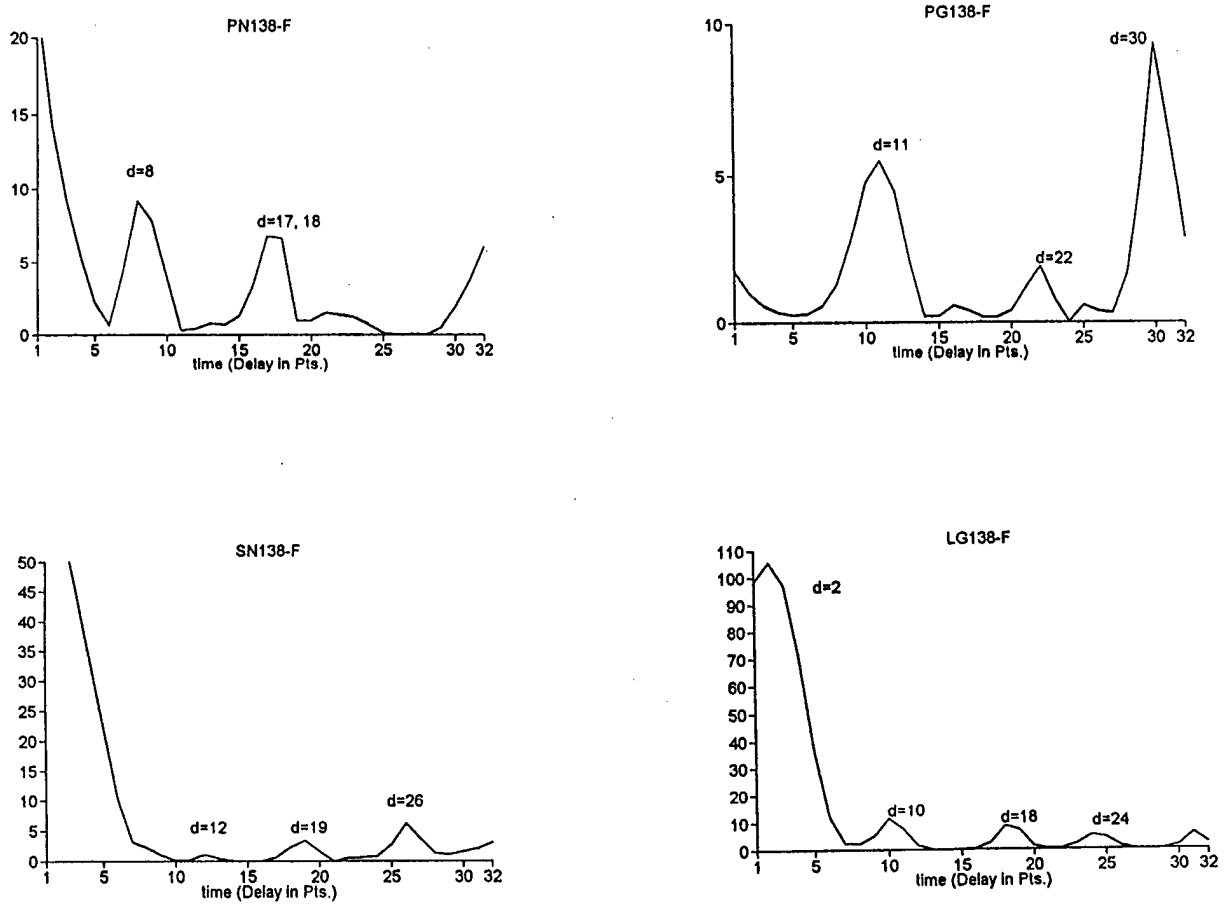

Figure A8: Cepstral F-Statistic for Four Phases From Event 138 (Delay in points).

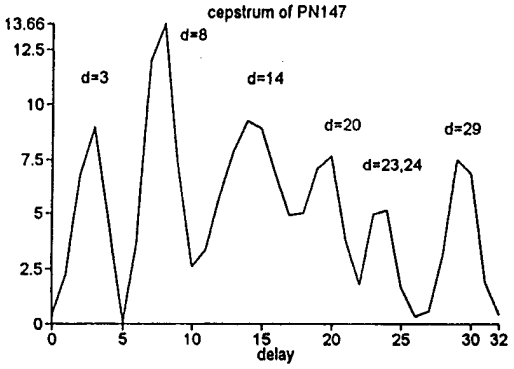

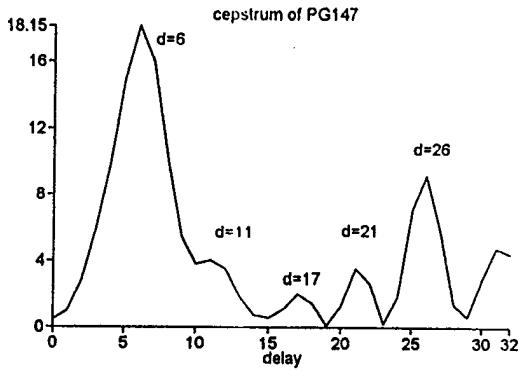

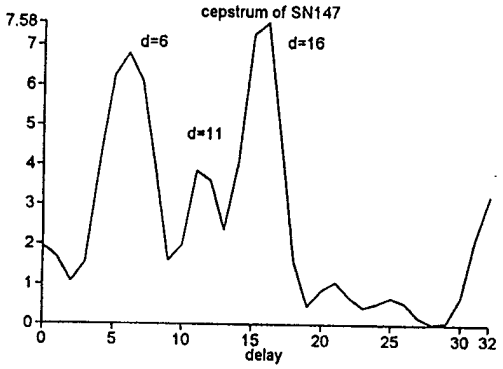

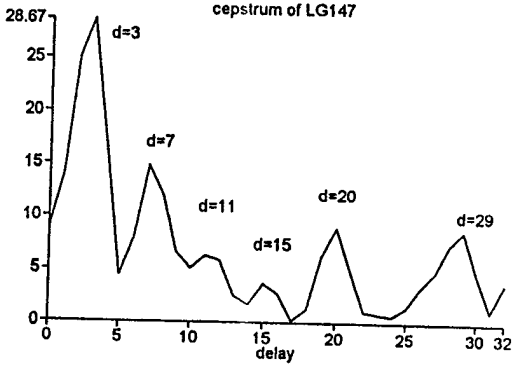

Figure A9: Cepstral Analysis of Deconvolved Array Signal for Four Phases From Event 147 (Delay in points).

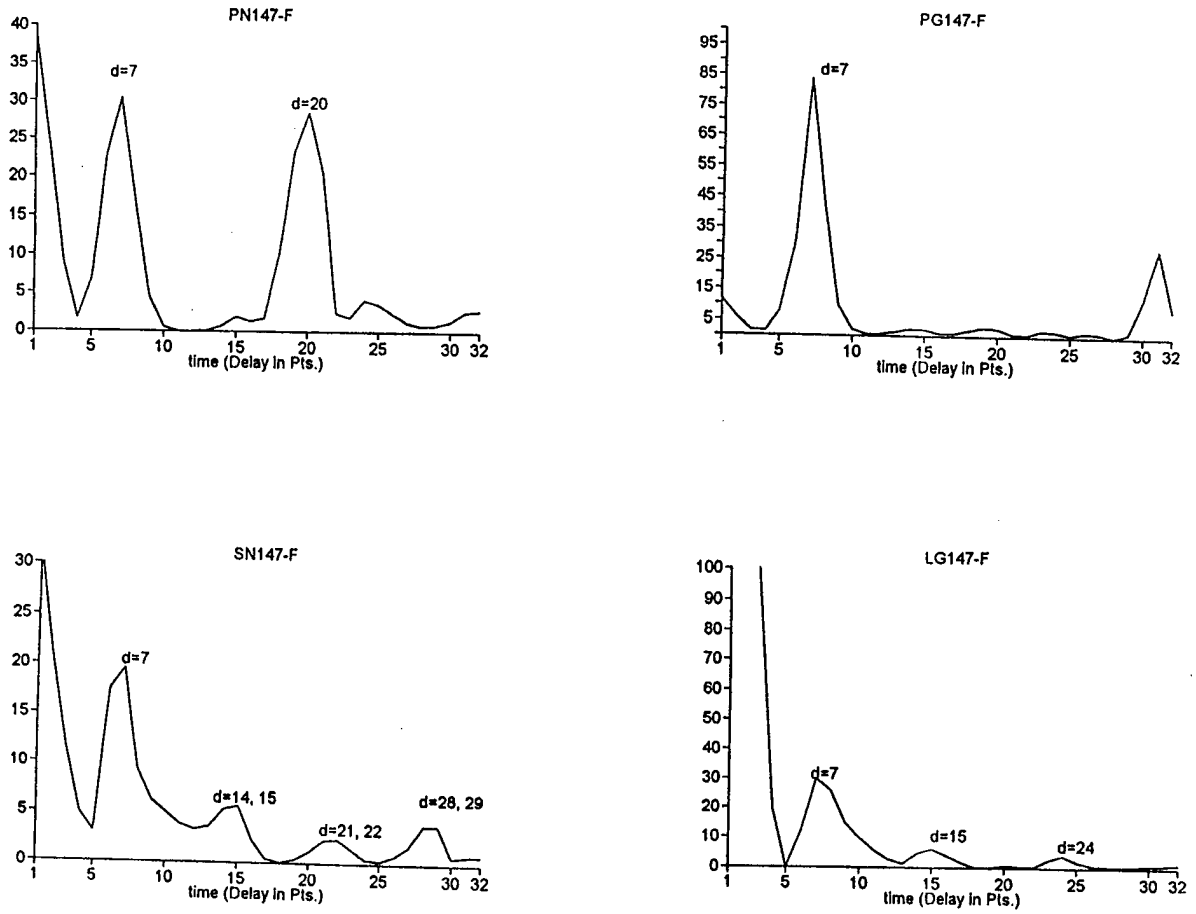

Figure A10: Cepstral F-Statistic for Four Phases From Event 147 (Delay in points).

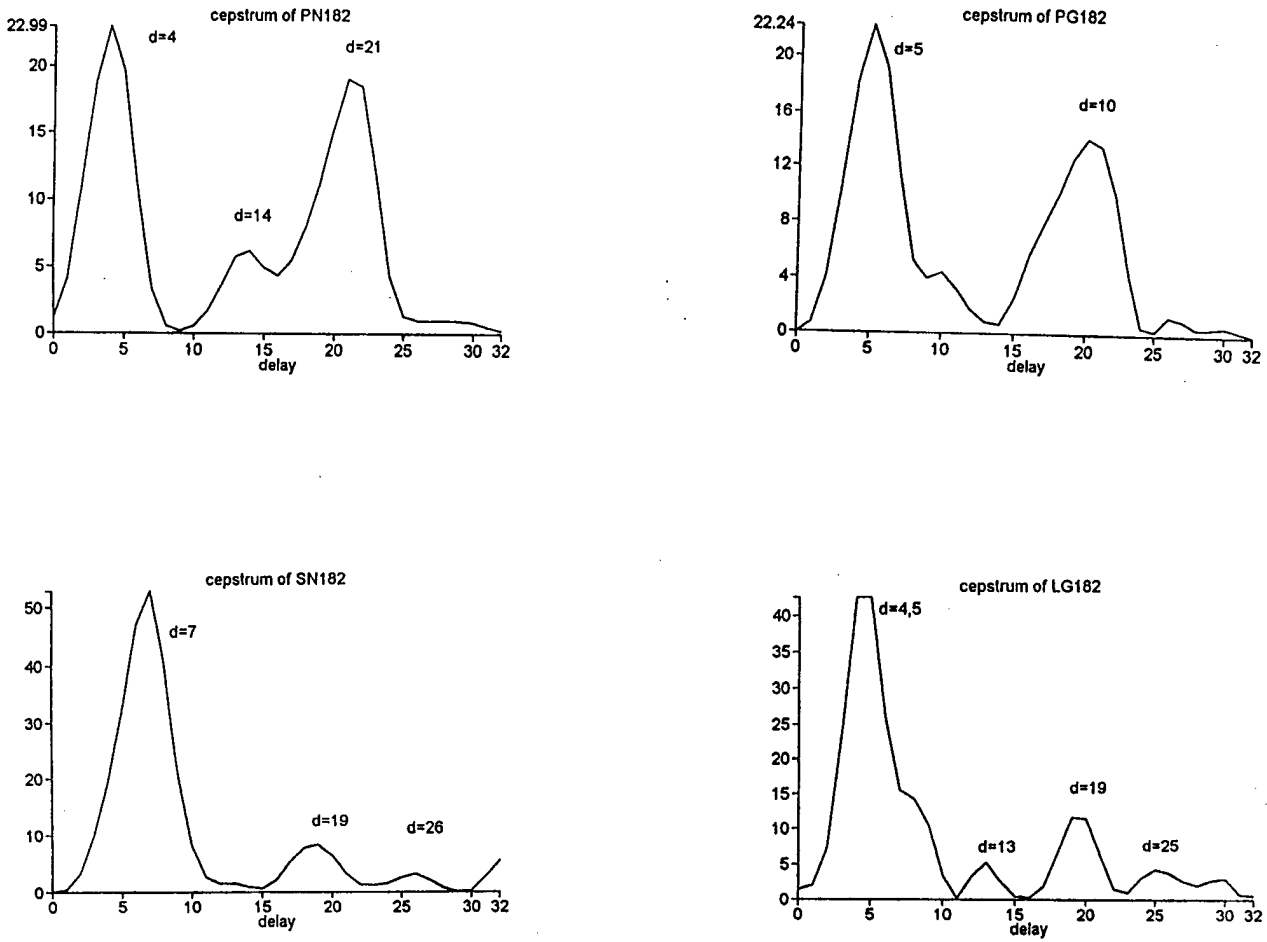

Figure A11: Cepstral Analysis of Deconvolved Array Signal for Four Phases From Event 182 (Delay in points).

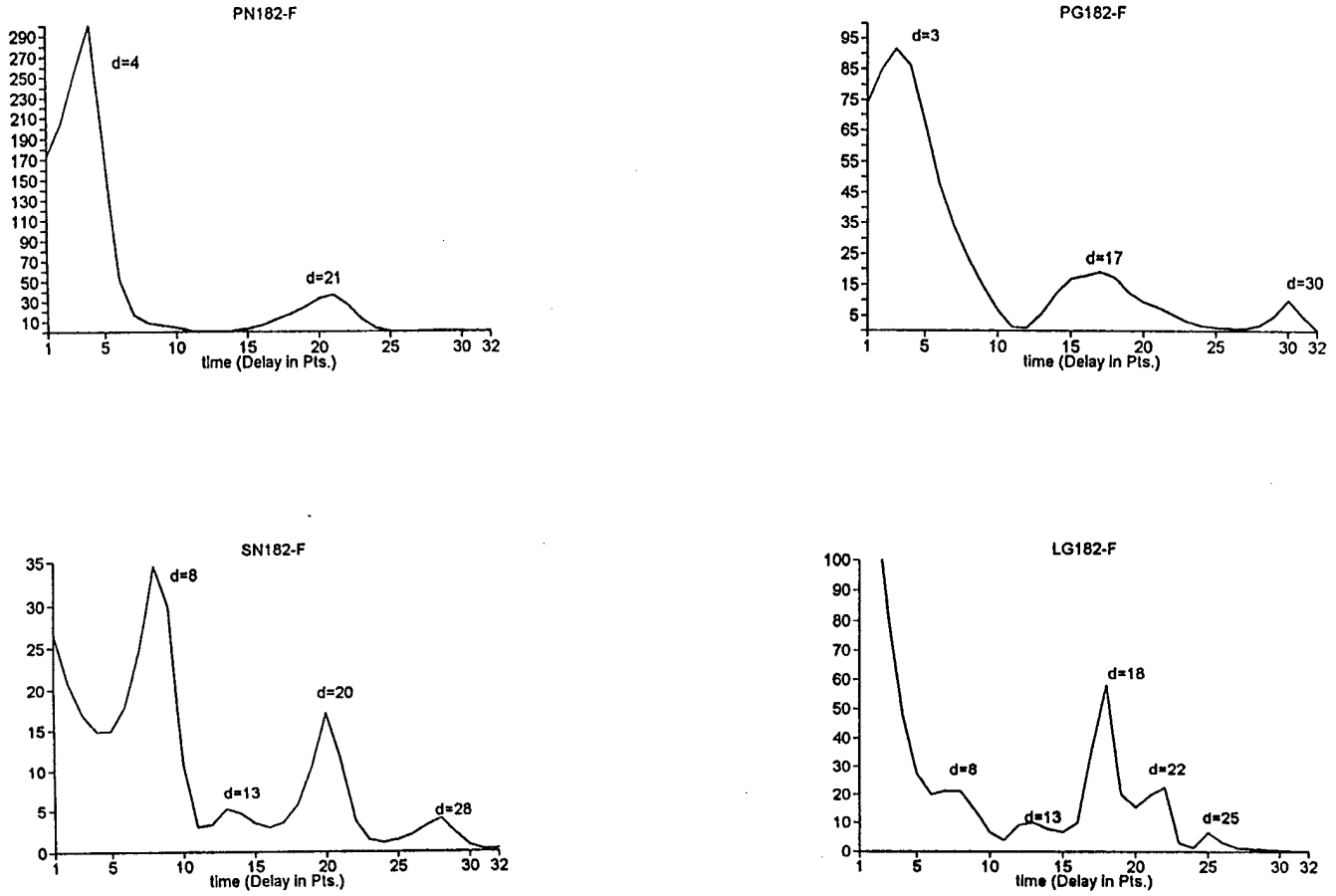

Figure A12: Cepstral F-Statistic for Four Phases From Event 182 (Delay in points).

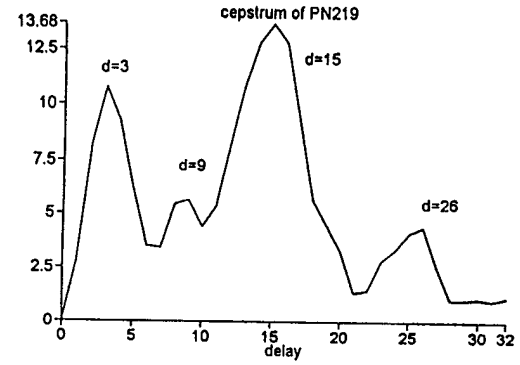

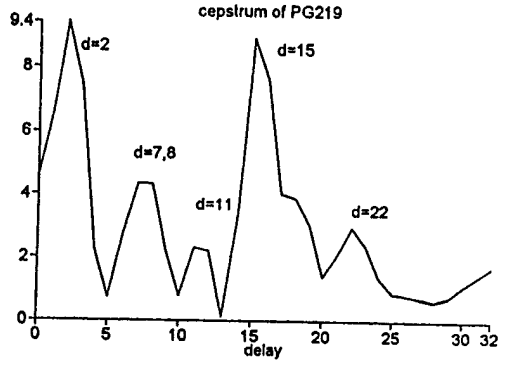

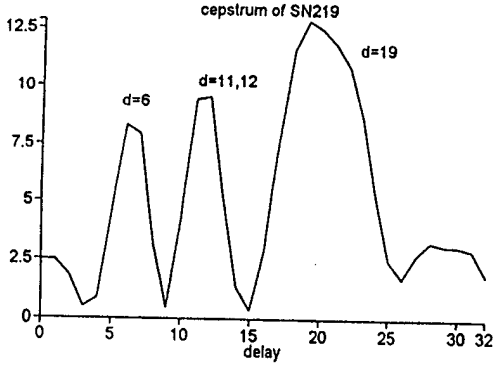

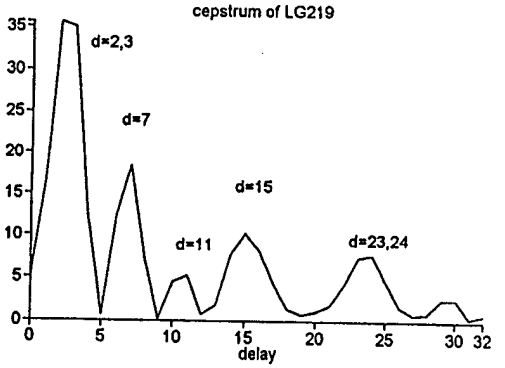

Figure A13: Cepstral Analysis of Deconvolved Array Signal for Four Phases From Event 219 (Delay in points).

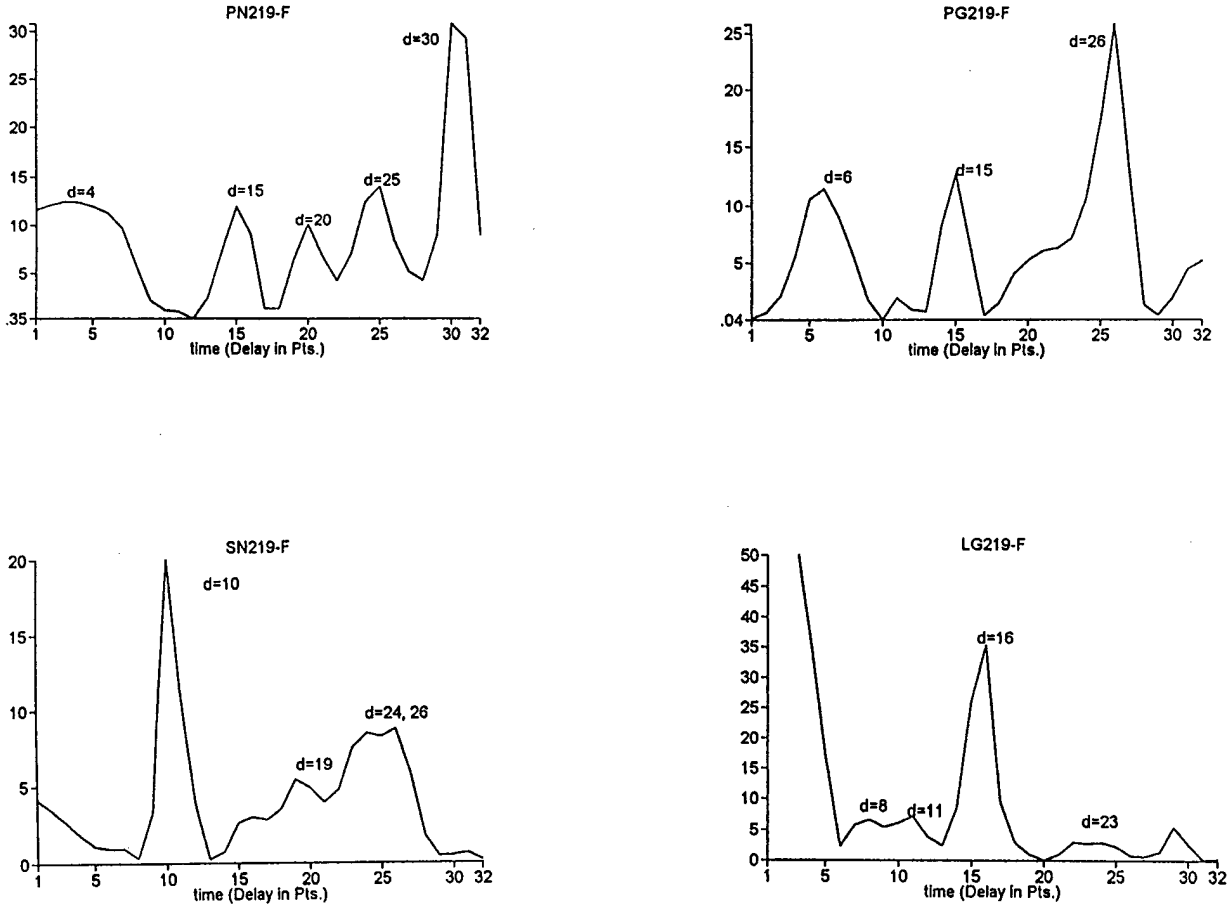

Figure A14: Cepstral F-Statistic for Four Phases From Event 219 (Delay in points).

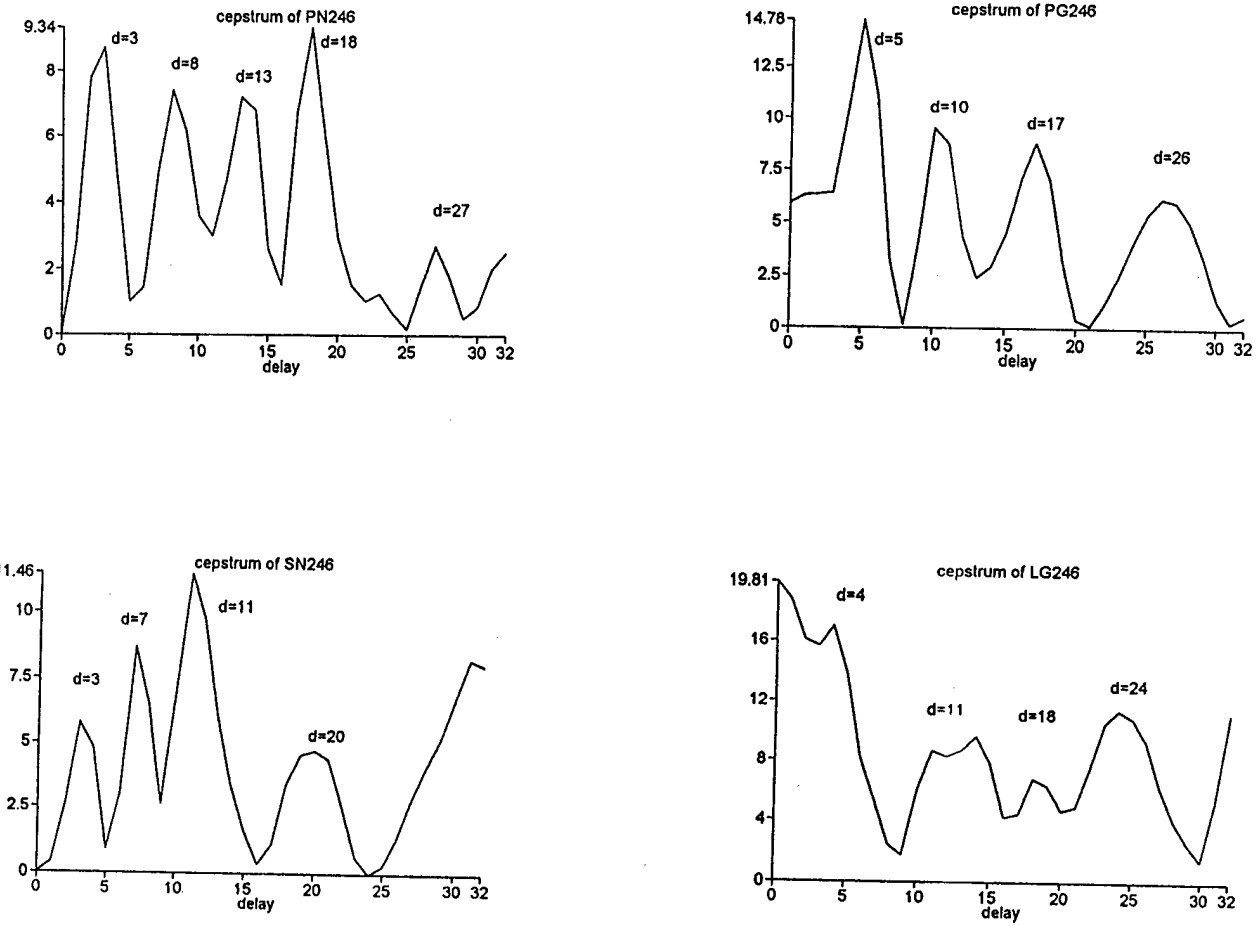

Figure A15: Cepstral Analysis of Deconvolved Array Signal for Four Phases From Event 246 (Delay in points).

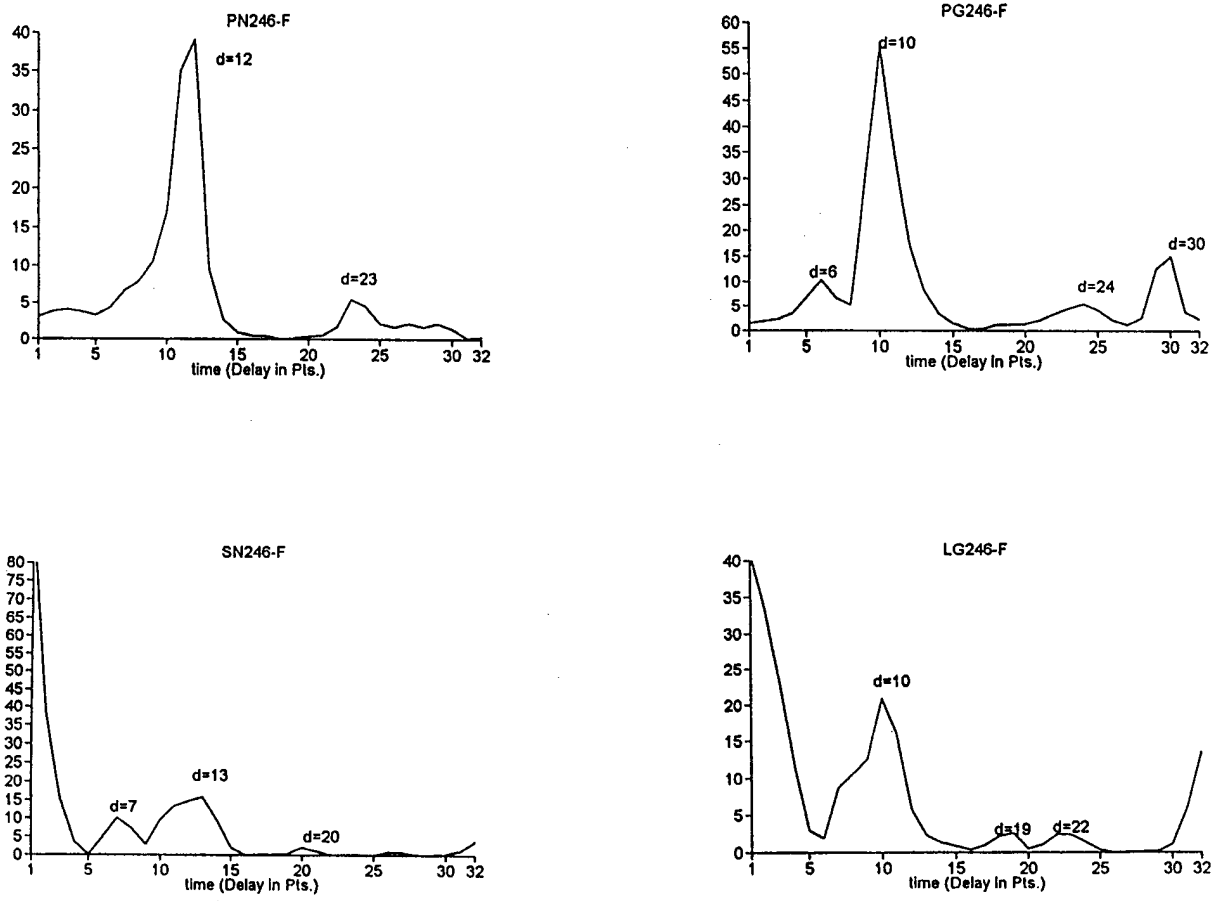

Figure A16: Cepstral F-Statistic for Four Phases From Event 246 (Delay in points).

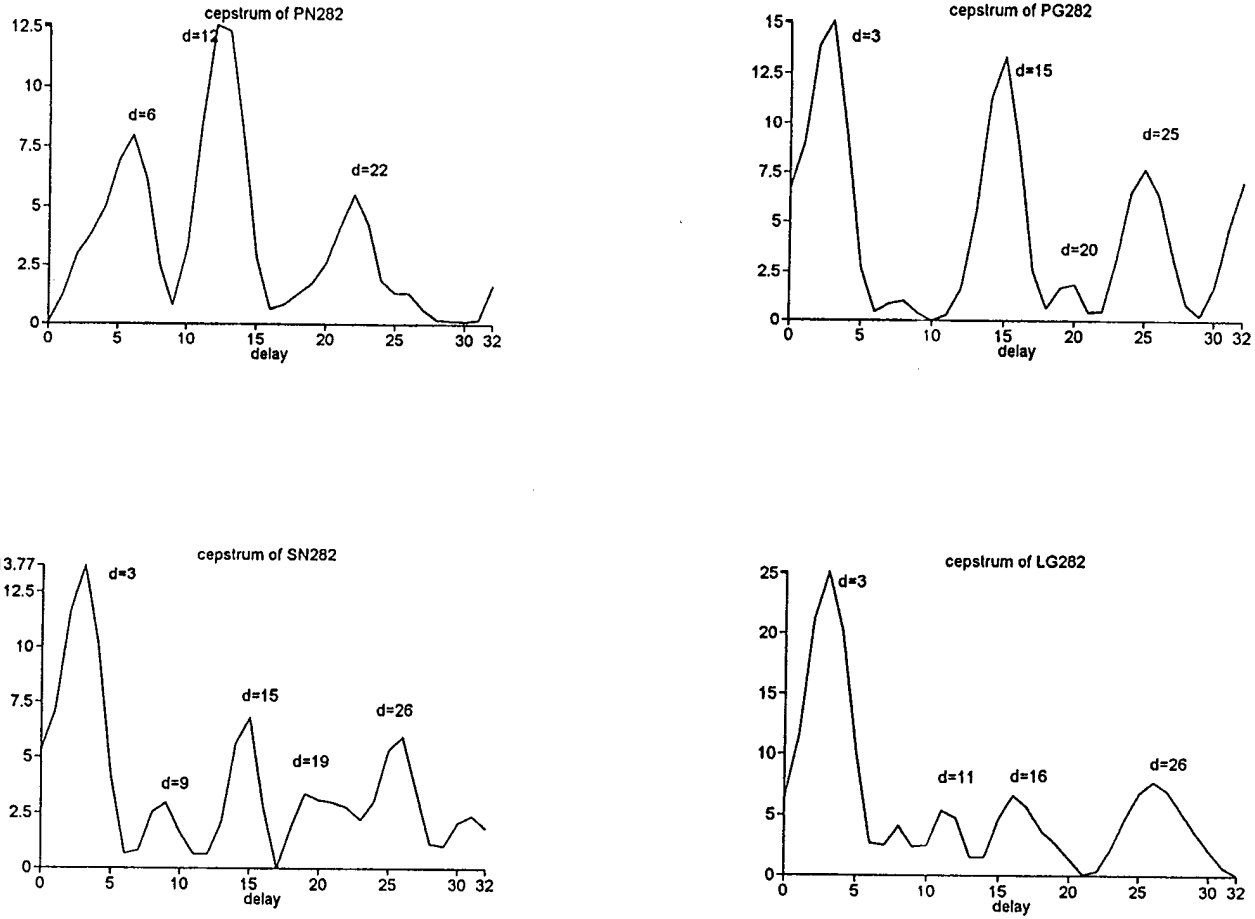

Figure A17: Cepstral Analysis of Deconvolved Array Signal for Four Phases From Event 282 (Delay in points).

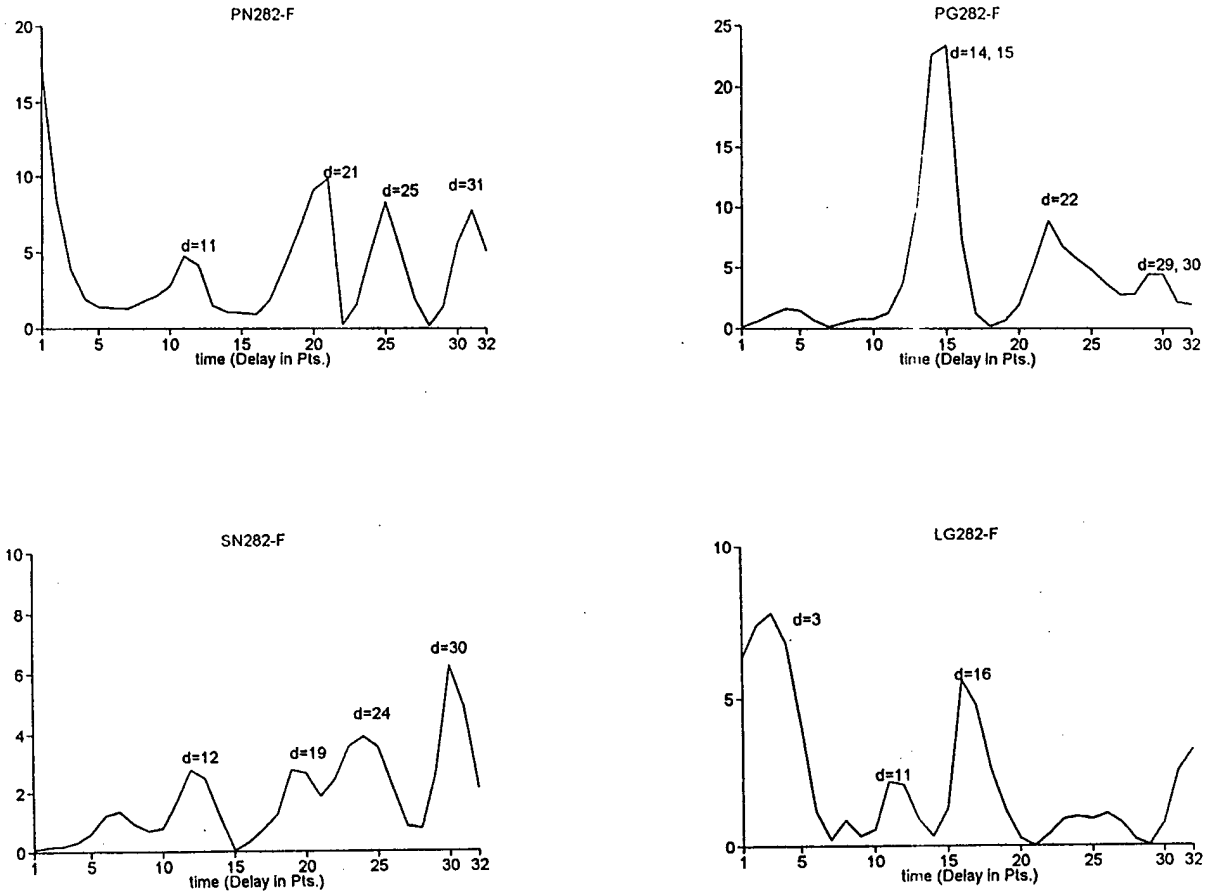

Figure A18: Cepstral F-Statistic for Four Phases From Event 282 (Delay in points).

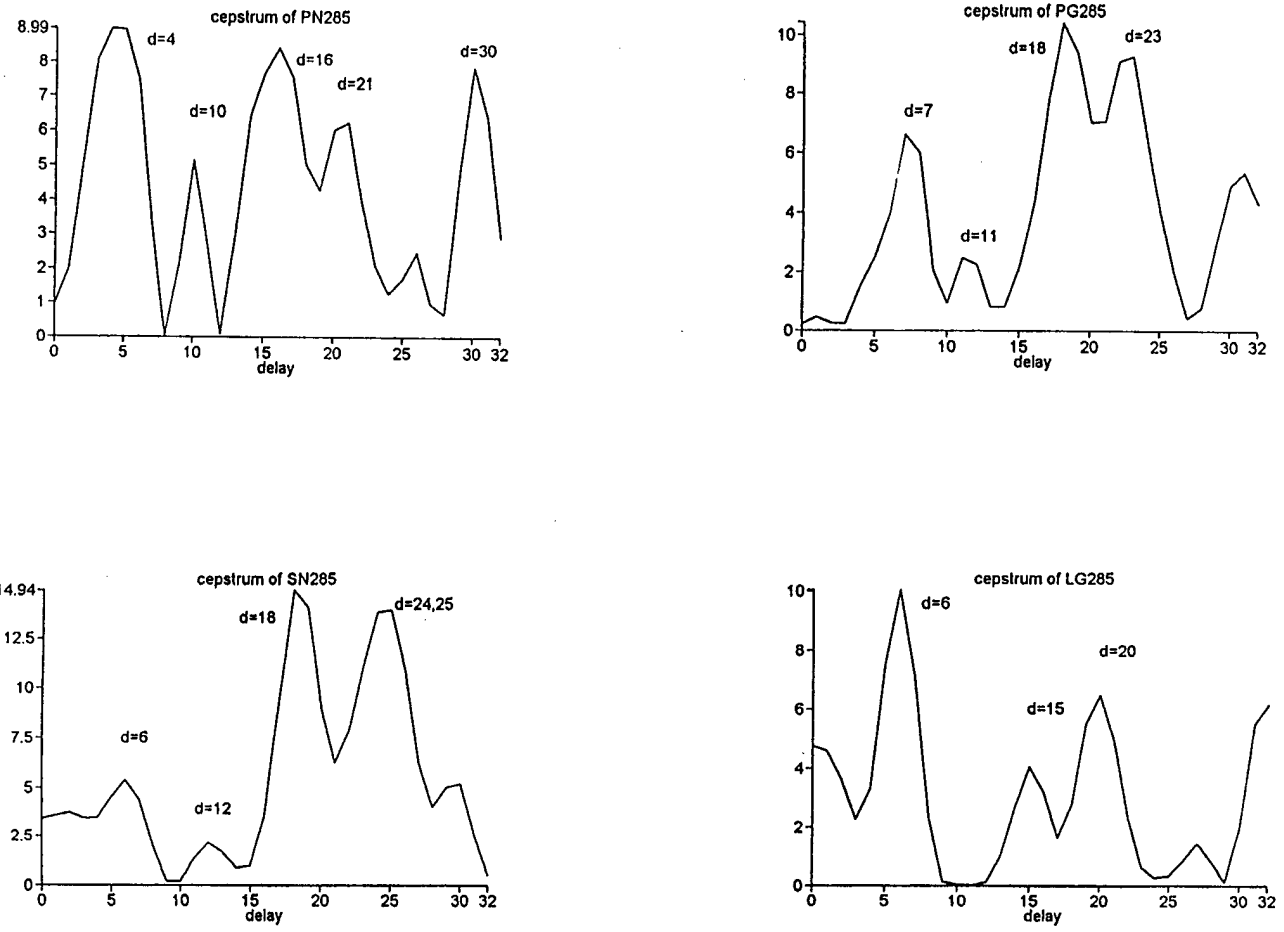

Figure A19: Cepstral Analysis of Deconvolved Array Signal for Four Phases From Event 285 (Delay in points).

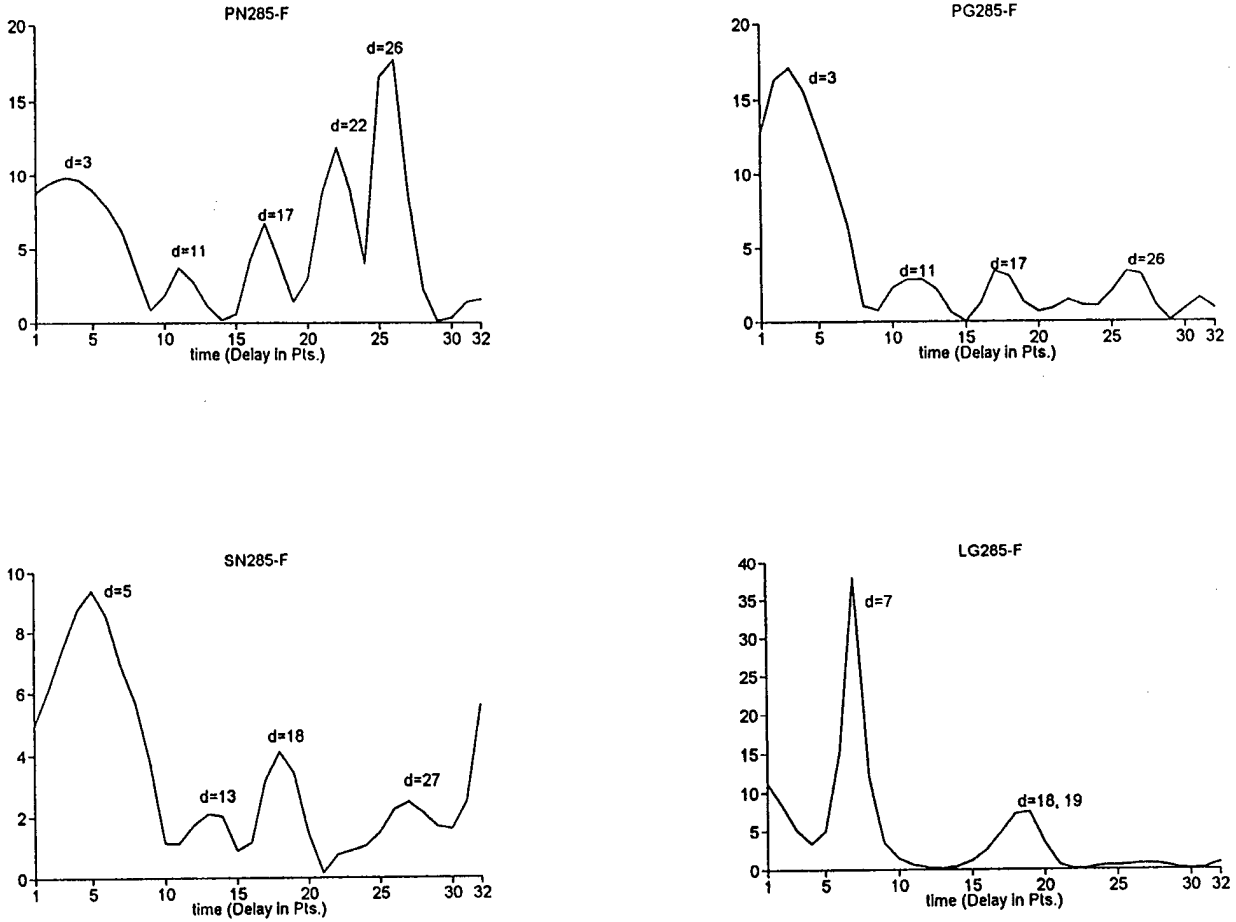

Figure A20: Cepstral F-Statistic for Four Phases From Event 285 (Delay in points).